

Double Machine Learning for Time Series

MILOS CIGANOVIC[†], FEDERICO D'AMARIO[†] AND MASSIMILIANO TANCIONI[†]

[†]*Sapienza University of Rome*

*E-mail: milos.ciganovic@uniroma1.it; federico.damario@uniroma1.it;
massimiliano.tancioni@uniroma1.it*

Summary We modify the Double Machine Learning estimator to broaden its applicability to macroeconomic time-series settings. A deterministic cross-fitting step, termed Reverse Cross-Fitting, leverages the time-reversibility of stationary series to improve sample utilization and efficiency. We detail and prove the conditions under which the estimator is asymptotically valid. We then demonstrate, through simulations, that its performance remains valid in realistic finite samples and is robust to model misspecification and violations of assumptions, such as heteroskedasticity. In high dimensions, predictive metrics for tuning nuisance learners do not generally minimize bias in the causal score. We propose a calibration rule targeting a “Goldilocks zone”, a region of tuning parameters that delivers stable, partialled-out signals and reduced small-sample bias. Finally, we apply our procedure to residualized Local Projections to estimate the dynamic effects of a rise in Tier 1 regulatory capital. The results underscore the usefulness of the methodology for inference in macroeconomic applications.

Keywords: *Causal Inference, Double Machine Learning, Time Series, Cross-Fitting, Hyperparameters tuning, Local Projections.*

1. INTRODUCTION

The recently developed Double/Debiased Machine Learning (DML) estimator (Chernozhukov et al., 2018) provides a valid alternative to standard causal inference methods for microeconomic data (Ahrens et al., 2025). Building on Robinson (1988)’s partially linear regression (PLR) model, it identifies a low-dimensional causal parameter while controlling for potentially high-dimensional, nonlinear confounders. These nuisance functions, though not of direct interest, must be accurately approximated using modern Machine Learning (ML) methods to ensure valid inference. DML aims to reduce the target parameter estimate’s sensitivity to approximation error in these functions. Robustness is achieved through Neyman orthogonalization, which removes regularization bias, and randomized cross-fitting (CF), which alternately assigns folds as training and test samples, mitigating overfitting and improving efficiency in i.i.d. settings.

This paper examines the applicability of DML to macroeconomic time series, which are typically short, strongly dependent, and highly endogenous. Such features can create high-dimensional settings where the parameter space may exceed the sample size. Standard DML, designed for independent observations, cannot yield valid inference in this context, as randomized cross-fitting would violate the series’s sequential structure.

By modifying specific features of DML, we establish its validity for time-dependent data. The adapted estimator has two key components. First, a novel Reverse Cross-Fitting (RCF) procedure leverages the time-reversibility of stationary Gaussian processes to improve sample usage and enhance efficiency in realistic time-dependent samples. Second, we introduce a fold-specific, stability-based calibration for nuisance learners, replacing standard predictive tuning. This criterion identifies a “Goldilocks zone” of

tuning parameters in which the fold-specific RMSE varies minimally. Consistent with Neyman orthogonality, estimates within this stability region achieve minimal bias, a property that may fail when using predictive metrics in high-dimensional control settings (McGrath et al., 2025).

To parallel the plain DML framework, we express the time-series inference problem using the PLR model of Robinson (1988), as in Chernozhukov et al. (2018). We aim for root- T -consistent estimation and valid inference for a low-dimensional causal parameter θ_0 in the presence of high-dimensional controls and nuisance functions $\eta_0 = (m_0, g_0)$:

$$y_t = \theta_0 d_t + g_0(X_t) + \epsilon_t, \quad E[\epsilon_t | X_t, d_t] = 0, \quad (1.1)$$

$$d_t = m_0(X_t) + \xi_t, \quad E[\xi_t | X_t] = 0. \quad (1.2)$$

where y_t is the outcome, d_t a scalar policy variable, $X_t = (X_1, \dots, X_p)$ the vector of controls, and ϵ_t and ξ_t disturbances, for $t = 1, \dots, T$.

Belloni et al. (2014) propose the post-double-selection procedure, which substantially reduces regularization bias by applying Lasso to both the reduced-form of (1.1) and (1.2) and regressing y_t on d_t and the union of selected controls.¹

Chernozhukov et al. (2018) extend this approach to settings with highly complex, non-linear nuisance functions via DML, allowing valid inference with general ML learners. Relative to post-double-selection, DML introduces three core elements: (i) Neyman orthogonalization, which removes regularization bias by forming a residualized outcome and policy equation from the reduced-form outcome equation $y_t = g_0^r(X_t) + \chi_t$, with $g_0^r \neq g_0$, and the policy equation (1.2)

$$\chi_t = \theta_0 \xi_t + \epsilon_t, \quad (1.3)$$

so that applying OLS to residuals accommodates unspecific ML estimators for g_0^r and m_0 ; (ii) sample splitting, which separates data used to learn nuisance functions from data used to estimate θ_0 and mitigates overfitting; and (iii) cross-fitting (CF), which alternates the roles of training and test sets to restore efficiency and full sample usage.

While the first two features transfer naturally to time-series applications, standard CF does not, as it relies on independence across folds. Random splitting would violate the temporal dependence structure, motivating the need for a time-series-adapted CF procedure.

To handle temporal dependence in microeconomic DML applications, Semenova et al. (2023) propose the Neighbours-Left-Out (NLO) CF procedure for weakly dependent panel data. NLO exploits the mixing properties of the series by partitioning data into blocks and omitting neighboring observations to create quasi-independent folds. For typical macroeconomic time series, achieving approximate independence requires substantial truncation, reducing sample efficiency. We introduce RCF to address this limitation.

We structure the analysis in three steps. We begin by detailing the time-series RCF-DML estimator and outlining the conditions for achieving asymptotic minimum-bias properties and efficiency with generic ML learners. A key focus is on conditional stability, a time-series-specific requirement preventing block dependence from reintroducing bias, akin to a “no data leakage” condition. Under this and standard DML conditions, the estimator is asymptotically consistent, with variance converging to an absolutely summable long-run variance, which can be consistently estimated using HAC corrections.

¹Naively applying selection methods to (1.1) may discard controls with coefficients “moderately close to zero,” inducing omitted-variable (regularization) bias (Belloni et al., 2014)

Next, we conduct extensive simulations based on approximately sparse (Giannone et al., 2021) structural VAR and PLR DGPs, leveraging a recursivity assumption for the contemporaneous structure.² The results indicate that RCF-DML delivers root- T -consistent estimates with coverage levels approaching nominal rates even under model mis-specification.³ In realistic finite samples, the RCF strategy outperforms NLO, especially in scenarios with strong persistence.

The finite sample simulations also reveal challenges in applying RCF-DML to real data. Standard predictive tuning, common in forecasting and causal ML, does not minimize bias, particularly as dimensionality increases relative to sample size. In these regimes, the divergence between minimum-bias MSE and predictive MSE increases.⁴ This result is consistent with recent findings (Celentano and Wainwright, 2023; McClean et al., 2024; McGrath et al., 2025). To address this issue, we propose a stability-based tuning criterion that targets a Goldilocks zone of tuning parameters, producing minimal fold-specific RMSE variation. Importantly, RMSE itself need not be minimal across the tested calibrations. This logic parallels sufficient-variability requirements in IV identification (Jaeger, 1995) applied to ML-residualized second-stage regressions (Athey and Wager, 2019).

Notably, RCF-DML remains low-bias even when the recursivity assumption is violated, inducing mis-specification in contemporaneous controls. Moreover, by incorporating GARCH dynamics into the SVAR DGP, we demonstrate robustness to severe non-normality, which violates time reversibility. In small samples, the bias advantages of RCF-DML outweigh efficiency losses relative to time-directional CF strategies.

Additionally, we show that, in a dynamic setting, nuisance-function residuals can be utilized to construct unbiased structural impulse responses via residualized Local Projections (DML-LPs). Under conditional unconfoundedness, supported by high-dimensional conditioning, the time-series-adapted DML estimator provides a new framework for identifying macroeconomic shocks and tracing their transmission.

Finally, we apply our method to estimate the dynamic effects of prudential capital shocks, a context well-suited for RCF-DML, given the short time span of regulatory data. The results align closely with consensus findings from established identification strategies.

Our analysis contributes to the growing literature on ML-assisted causal inference (Athey and Imbens, 2016; Athey et al., 2019; Chernozhukov et al., 2018). Within the DML framework, we relate to recent work on cross-sectional and panel data (Ahrens et al., 2025; Chang, 2020; Chernozhukov et al., 2022b,a; Dube et al., 2020; Semenova and Chernozhukov, 2021; Semenova et al., 2023). In macroeconomic applications, our approach complements Adamek et al. (2024), who use desparsified Lasso for high-dimensional time-series LPs, and Agostini et al. (2024), who apply dynamic DML-type residualization to panel-data LPs. Regarding learner calibration, our results echo recent work highlighting that optimal tuning for DML inference differs from predictive optimality. McClean et al. (2024) advocate undersmoothing to improve convergence, while McGrath et al. (2025)

²For tractability, nuisance functions are estimated using linear ML methods. The DML framework also accommodates nonlinear learners such as random forests, boosting, neural networks, and ensembles.

³Model mis-specification is introduced by considering all the variables as contemporaneous, even if the true DGP is recursive.

⁴This divergence echoes Robinson (1988)'s findings on allowable kernel complexity in its prototypical PLR. The issue is independent of the CF design and not attributable to failures in relaxing Donsker conditions.

demonstrate that in high-dimensional (inconsistency) regimes, minimum bias is achieved by minimizing the asymptotic variance of the target functional.

The remainder of the paper is structured as follows. Section 2 introduces RCF and the notion of time reversibility, proving that, under suitable conditions, RCF-DML is asymptotically consistent and efficient. Section 3 introduces the Goldilocks zone tuning strategy and explains its role in bias control for high-dimensional time series. Section 4 presents the simulation results. Section 5 provides an empirical application. Section 6 concludes.

2. INFERENCE WITH REVERSE CROSS-FITTING

Cross-fitting restores efficiency after sample splitting by alternating the roles of training and test sets. In i.i.d. settings, this is achieved through random partitioning. However, random splitting is infeasible for time series because it breaks the temporal dependence structure.

We propose the RCF method as an alternative CF strategy for time series, tailored to macroeconomic data. Rather than enforcing independence across folds, RCF exploits the time-reversibility of stationary processes to construct auxiliary and main samples that preserve the temporal structure while maximizing sample usage. This design avoids the truncation costs of NLO and provides an efficiency-preserving cross-fitting scheme.

A stochastic process X_t is time-reversible if, for any window length D , the joint distributions of $X_t = \{X_t, X_{t+1}, \dots, X_{t+D}\}$ and of its time-reversed version, $X'_t = \{X_{t+D}, X_{t+D-1}, \dots, X_t\}$ are identical for all t . All stationary Gaussian processes, and nonlinear transformations of them, are time-reversible because their joint distributions depend only on the symmetric covariance function (Weiss, 1975; Hallin et al., 1988).⁵

2.1. The mechanics of time-Reversed Cross-Fitting

Consider a partition of the set $\{1, \dots, T\}$ into adjacent blocks $\{\mathcal{B}_k\}_{k=1}^K$, each of equal length (i.e. $T_k = T_{\text{block}} = \lfloor \frac{T}{K} \rfloor$). For any k , define the left and right index sets:

$$L(k) = \{1, \dots, k\}, \quad R(k) = \{k, \dots, K\}.$$

and the corresponding left- and right-“complements” of \mathcal{B}_k as:

$$\mathcal{B}_k^L = \{\mathcal{B}_1, \dots, \mathcal{B}_K\} \setminus \{\mathcal{B}_i : i \in R(k)\}, \quad \mathcal{B}_k^R = \{\mathcal{B}_1, \dots, \mathcal{B}_K\} \setminus \{\mathcal{B}_i : i \in L(k)\}.$$

Let the associated data blocks be:

$$D_k = \{W_{\cdot,t} : t \in \mathcal{B}_k\}, \quad D_{L,k} = \{W_{\cdot,t} : t \in \mathcal{B}_k^L\}, \quad D_{R,k} = \{W_{\cdot,t} : t \in \mathcal{B}_k^R\}.$$

Consider $K = 5$, defining corresponding blocks $\{\mathcal{B}_k\}_{k=1}^5$ of adjacent time stamps $t \in \{1, \dots, T\}$, each of size T_{block} , so that $T = KT_{\text{block}}$. The partition defines five non-overlapping blocks \mathcal{B}_k , considered as main sets in the five-fold-RCF, and left- and right-complementary blocks, which are auxiliary sets: $\mathcal{B}_1^L = \emptyset$, $\mathcal{B}_1^R = \{\mathcal{B}_k\}_{k=2}^5$; $\mathcal{B}_2^L = \mathcal{B}_1$,

⁵The PLR model allows nonlinear nuisance functions; under time reversibility, reversing the series does not affect the model parameters. Cheng (1999) provides necessary and sufficient conditions for the reversibility of stationary linear processes without requiring higher-order moments, and Tong and Zhang (2005) extends these results to the multivariate case, covering many non-Gaussian stationary linear processes. Time reversibility is statistically testable. For zero-mean series, Ramsey’s test (Rothman, 1990) exploits the symmetry of differences of reversible processes by comparing sample bi-covariances at lag (τ), i.e., $\gamma(\tau) = \{X_t^2 X_{t-\tau}\} - \{X_{t-\tau}^2 X_t\}$. Martínez et al. (2018) propose the TiROP test, which relies on ordinal patterns and makes no moment assumptions.

$\mathcal{B}_2^R = \{\mathcal{B}_k\}_{k=3}^5$; $\mathcal{B}_3^L = \{\mathcal{B}_k\}_{k=1}^2$, $\mathcal{B}_3^R = \{\mathcal{B}_k\}_{k=4}^5$; $\mathcal{B}_4^L = \{\mathcal{B}_k\}_{k=1}^3$, $\mathcal{B}_4^R = \mathcal{B}_5$; $\mathcal{B}_5^L = \{\mathcal{B}_k\}_{k=1}^4$, $\mathcal{B}_5^R = \emptyset$. Nuisance functions are therefore estimated in time-reversed mode in the first two folds, in forward mode in the last two, and in both directions in the central fold.

In typical macroeconomic samples, auxiliary blocks adjacent to the main block, e.g., the second-left or fourth-right block, may contain too few observations. Including such blocks leads to nuisance estimates dominated by very short segments. In such cases, it is preferable to omit these undersized blocks from nuisance estimation. RCF addresses this by adopting an auxiliary-set rule, dropping the smaller side of the auxiliary sample: $D_{\text{aux},k} = D_{L,k}$ if $|D_{L,k}| < |D_{R,k}|$, $D_{\text{aux},k} = D_{R,k}$ if $|D_{R,k}| < |D_{L,k}|$, and $D_{\text{aux},k} = D_{L,k} \cup D_{R,k}$ if $|D_{L,k}| = |D_{R,k}|$. For any $K \geq 4$, the auxiliary sample used for fold k is therefore only left (backward) or only right (forward) if one side is smaller, both sides when k is central (odd K -fold CF), and the auxiliary blocks have equal size.

Figure 1 illustrates this five-fold Reverse Cross-Fitting scheme.

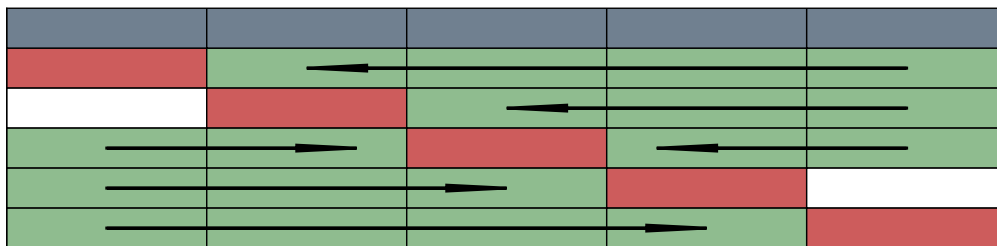


Figure 1. Example of Reverse Cross-Fitting using five folds. The Blue area represents the whole sample. Red blocks are "Main" observations. Green blocks are "Quasi-complementary" observations. White blocks represent left-out observations, and the direction of the arrows indicates the direction of the estimate.

To generalize across sample sizes, consider each fold as containing a single observation. RCF attains higher, equal, or lower usage than NLO when $K < 11$, $K = 11$, and $K > 11$, respectively. Under NLO, usage exceeds 70% for $K \geq 10$. Using many folds in macroeconomic time series reduces the size of the left-out blocks and may violate weak dependence assumptions. By providing higher usage for all $K < 11$, RCF offers a practical advantage in small samples.

2.2. The RCF-DML estimator

Let $(W_t)_{t=1}^T$ be a covariance-stationary, ergodic time series on $(\Omega, \mathcal{F}, \mathbb{P})$. DML targets a finite-dimensional parameter $\theta_0 \in \Theta \subset \mathbb{R}^d$ while controlling for (possibly high-dimensional) nuisance objects η_0 . Let $\psi : \mathcal{W} \times \Theta \times \mathcal{H} \rightarrow \mathbb{R}^d$ be a score (moment) function satisfying Neyman orthogonality, i.e., the local invariance of θ_0 to errors in the approximation of η_0 :

$$\mathbb{E}[\psi(W_t; \theta_0, \eta_0)] = 0, \quad \partial_{\eta} \mathbb{E}[\psi(W_t; \theta_0, \eta)] \Big|_{\eta=\eta_0} = 0, \quad (2.4)$$

and let $A := \mathbb{E}[\partial_{\theta} \psi(W_t; \theta_0, \eta_0)]$ be nonsingular. Partition the index set $\{1, \dots, T\}$ into K adjacent, non-overlapping blocks $\{B_k\}_{k=1}^K$, each of length $|B_k| = \lfloor T/K \rfloor$ up to $O(1)$

boundary effects. For each main block B_k , define its left and right complements

$$B_k^L := \bigcup_{i < k} B_i, \quad B_k^R := \bigcup_{i > k} B_i.$$

RCF trains the nuisance function on data lying *outside* the main block. If $k < \lfloor K/2 \rfloor$, training is performed on B_k^R (using time-reversed future data). If $k > \lfloor K/2 \rfloor$, training is performed on B_k^L (using past data). If $k = \lfloor K/2 \rfloor$ and K is odd, both B_k^L and B_k^R are used. This scheme guarantees strict separation between training and main blocks.

Within B_k , use the nuisance estimates $\hat{\eta}^{(k)}$ to construct residualized outcome and policy series, $(\chi_{t,k}, \xi_{t,k})_{t \in B_k}$, and compute the residual-on-residual OLS slope

$$\hat{\theta}_k := \arg \min_{\theta \in \Theta} \frac{1}{|B_k|} \sum_{t \in B_k} (\chi_{t,k} - \theta \xi_{t,k})^2.$$

Equivalently, the fold-specific empirical moment condition satisfies:

$$\frac{1}{|B_k|} \sum_{t \in B_k} \psi(W_t; \hat{\theta}_k, \hat{\eta}^{(k)}) = 0.$$

The RCF-DML estimator averages the K fold-specific estimates:

$$\hat{\theta} := \frac{1}{K} \sum_{k=1}^K \hat{\theta}_k. \quad (2.5)$$

2.3. Assumptions for valid inference

Define the oracle score $\psi_t^* := \psi(W_t; \theta_0, \eta_0)$, the lag- h autocovariance $\Gamma(h) := \text{Cov}(\psi_t^*, \psi_{t-h}^*)$, and the long-run variance

$$\Sigma := \sum_{h=-\infty}^{\infty} \Gamma(h), \quad \sum_h \|\Gamma(h)\| < \infty \text{ (ensures finiteness)}, \quad (2.6)$$

where the matrix Σ is the time-series analogue of $\text{Var}(\psi_t^*)$ in the i.i.d. case.

The RCF-DML estimator does not assume independence between auxiliary and main blocks. The following assumptions are required for valid inference.

ASSUMPTION 2.1. (FINITE HAC VARIANCE) $\mathbb{E}\|\psi_t^*\|^2 < \infty$ and Σ in (2.6) exists and is finite (equivalently $\sum_h \|\Gamma(h)\| < \infty$).

Assumption 2.1 ensures the oracle score has finite variance and that serial dependence is weak enough for a well-defined long-run variance. This assumption guarantees that the long-run variance exists and can be estimated with HAC methods. It excludes explosive or infinite-variance processes.

ASSUMPTION 2.2. (INVARIANCE PRINCIPLE FOR THE ORACLE SCORE) *In the full sample space $D([0, 1]; \mathbb{R}^d)$,*

$$\frac{1}{\sqrt{T}} \sum_{t=1}^{\lfloor uT \rfloor} \psi_t^* \Rightarrow \mathcal{W}(u),$$

where \mathcal{W} is a mean-zero Gaussian process with $\mathbb{E}[\mathcal{W}(u)\mathcal{W}(v)^\top] = (u \wedge v) \Sigma$.

Assumption 2.2 is the functional central limit theorem (FCLT): the partial-sum process of the oracle scores $\psi_t^* = \psi(W_t; \theta_0, \eta_0)$, normalized by \sqrt{T} , converges weakly in the space $D([0, 1]; \mathbb{R}^d)$ to a multivariate Brownian motion with covariance kernel $(u \wedge v)\Sigma$.⁶ This FCLT yields the asymptotic normality of the RCF–DML estimator, which considers time-dependent stationary series (see, e.g., Billingsley 1968; Hansen 1982; Herrndorf 1984). Sufficient conditions for Assumption 2.2 include the Maxwell–Woodroffe projective criterion (Maxwell and Woodroffe 2000) and, more generally, summable α -mixing.⁷ Using this framework, in the supplementary appendix, we verify Assumption 2.2 for the DGPs considered in the paper.

ASSUMPTION 2.3. (SMOOTHNESS AND NEYMAN ORTHOGONALITY)

(i) **Differentiability and orthogonality:** $\psi(W; \theta, \eta)$ is Gateaux-differentiable in (θ, η) near (θ_0, η_0) with integrable derivatives. It admits an L_2 expansion in η with a quadratic remainder:

$$\psi(W; \theta_0, \hat{\eta}) - \psi(W; \theta_0, \eta_0) = \partial_\eta \psi(W; \theta_0, \eta_0)[\hat{\eta} - \eta_0] + r(W; \hat{\eta}, \eta_0),$$

with $\mathbb{E}[r^2] \lesssim \|\hat{\eta} - \eta_0\|_{L_2}^4$. Moreover, $\mathbb{E}[\partial_\eta \psi(W; \theta_0, \eta_0)[h]] = 0$ for all admissible directions h (Neyman orthogonality).

(ii) **Derivative stationarity:** The derivative processes $\partial_\theta \psi(W_t; \theta_0, \eta_0)$ and $\partial_\eta \psi(W_t; \theta_0, \eta_0)$ are covariance-stationary with finite second moments and summable autocovariances:

$$\mathbb{E}\|\partial_\theta \psi(W_t; \theta_0, \eta_0)\|^2 < \infty, \quad \sum_h \|\Gamma_{\partial_\theta \psi}(h)\| < \infty,$$

where $\Gamma_{\partial_\theta \psi}(h) := \text{Cov}(\partial_\theta \psi(W_t; \theta_0, \eta_0), \partial_\theta \psi(W_{t-h}; \theta_0, \eta_0))$; and similarly for $\partial_\eta \psi$ (using operator norm).

(iii) **Lipschitz continuity:** There exists $L < \infty$ such that for η, η' in a neighbourhood of η_0 and a.e. W ,

$$\|\partial_\theta \psi(W; \theta_0, \eta) - \partial_\theta \psi(W; \theta_0, \eta')\| \leq L\|\eta - \eta'\|_{L_2},$$

and similarly for $\partial_\eta \psi$ in operator norm.

Assumption 2.3 guarantees smooth, linearizable dependence of the score on (θ, η) and enforces Neyman orthogonality so that nuisance errors enter only at second order. Part (i) thus establishes that, if the nuisance is estimated sufficiently well, the approximation errors are asymptotically negligible at the \sqrt{T} scale. Part (ii) extends weak-dependence and continuity requirements to the score derivatives, allowing for valid Jacobian and variance calculations under serial correlation. Part (iii) ensures that score derivatives change continuously with the nuisance parameter, such that L_2 convergence of $\hat{\eta}^{(k)}$ translates to uniform convergence of the Jacobian matrix across folds.⁸

⁶Here $u, v \in [0, 1]$ denote rescaled time indices, representing fractions of the sample (e.g. $u = 0.5$ corresponds to the first half of the series), and $(u \wedge v)\Sigma$ is the covariance kernel of the limiting Brownian motion: the variance grows linearly with time (u), while Σ captures the contemporaneous dependence across the d components of the score vector.

⁷The Maxwell–Woodroffe condition guarantees the functional central limit theorem for a broad class of stationary sequences, and summable α -mixing implies the Maxwell–Woodroffe condition. Time-reversible processes fall within this class, as their stationarity and covariance symmetry ensure that the criterion is automatically satisfied.

⁸Notably, the summability of autocovariances parallels the HAC conditions in Andrews (1991) and holds automatically for mixing processes (Hansen 1982).

ASSUMPTION 2.4. (DEPENDENT CROSS-FIT ACCURACY AND CONDITIONAL STABILITY)
For each fold k ,

$$\|\hat{\eta}^{(k)} - \eta_0\|_{L_2} = o_p(T^{-1/4}), \quad \sup_k \|\hat{\eta}^{(k)}\| = O_p(1).$$

Let $\mathcal{F}_{\text{aux},k}$ be the σ -field generated by the auxiliary blocks used to train $\hat{\eta}^{(k)}$. Then

$$\left\| \mathbb{E} \left[\frac{1}{|B_k|} \sum_{t \in B_k} \{\psi(W_t; \theta_0, \hat{\eta}^{(k)}) - \psi(W_t; \theta_0, \eta_0)\} \mid \mathcal{F}_{\text{aux},k} \right] \right\| = o_p(T^{-1/2}).$$

Assumption 2.4 imposes the usual L_2 -consistency rate ($o_p(T^{-1/4})$) and uniform boundedness of fold-specific nuisance estimators. Moreover, it adds a *conditional stability* requirement: the block-average conditional plug-in bias, given the training data to obtain $\hat{\eta}^{(k)}$, is negligible at the \sqrt{T} scale, even though the auxiliary and main blocks belong to the same time-dependent series. This condition replaces the usual fold-independence assumption and is the sole RCF-specific condition that handles dependence between auxiliary and main blocks.

Intuitively, this means that training on auxiliary blocks, which are non-overlapping but adjacent to the main block, does not induce systematic bias in the scores computed on the main block. This condition is the time series analogue of the no-data-leakage principle in statistical learning. As long as each main block is excluded from the training set and the learner generalizes in L_2 , the condition is mild. We verify this requirement for the DGPs considered in the paper in the supplementary appendix.

REMARK 2.1. (ON NON-INDEPENDENCE) *Assumption 2.4 replaces fold independence: we allow dependence between $(W_t)_{t \in B_k}$ and the auxiliary data through the filtration $\mathcal{F}_{\text{aux},k}$, but require the conditional plug-in bias to be second order. If violated, one must discard additional neighbours (as in NLO).*

ASSUMPTION 2.5. (BLOCK CONSTRUCTION) *Blocks $\{B_k\}$ are adjacent, non-overlapping, and cover $\{1, \dots, T\}$ up to $o(T)$ edge corrections; auxiliary sets do not reuse indices in B_k .*

REMARK 2.2. (CHOICE OF K) *In small samples, the choice of K should balance main/auxiliary-block sizes and maximize sample usage. Considering the asymptotic limit, in our proofs, K is not allowed to grow with T , since in large samples the choice of K does not affect the properties of the RCF-DML estimator.*

2.4. Asymptotic properties

This subsection derives the asymptotic distribution of the RCF-DML estimator under time dependence. We show that the estimator admits an asymptotic linear representation with the oracle score, is \sqrt{T} -consistent and asymptotically normal, and that a HAC estimator of the long-run variance is consistent. These results imply valid inference without fold independence or temporal gaps between training and main blocks. We provide complete proofs of the results in Appendix A.

LEMMA 2.1. (ORTHOGONALITY REMAINDER UNDER DEPENDENCE) For each fold k , define the block-average discrepancy

$$R_k := \frac{1}{|B_k|} \sum_{t \in B_k} \left\{ \psi(W_t; \theta_0, \hat{\eta}^{(k)}) - \psi(W_t; \theta_0, \eta_0) \right\}.$$

Under Assumptions 2.3–2.4, $R_k = o_p(T^{-1/2})$ uniformly in k . Consequently,

$$\frac{1}{|B_k|} \sum_{t \in B_k} \psi(W_t; \theta_0, \hat{\eta}^{(k)}) = \frac{1}{|B_k|} \sum_{t \in B_k} \psi(W_t; \theta_0, \eta_0) + o_p(T^{-1/2}), \quad k = 1, \dots, K, \quad (2.7)$$

and the average over k also satisfies

$$\frac{1}{K} \sum_{k=1}^K \frac{1}{|B_k|} \sum_{t \in B_k} \psi(W_t; \theta_0, \hat{\eta}^{(k)}) = \frac{1}{K} \sum_{k=1}^K \frac{1}{|B_k|} \sum_{t \in B_k} \psi(W_t; \theta_0, \eta_0) + o_p(T^{-1/2}). \quad (2.8)$$

LEMMA 2.2. (PER-FOLD OLS LINEARIZATION) Let $\hat{\theta}_k$ satisfy the fold moment equation $\frac{1}{|B_k|} \sum_{t \in B_k} \psi(W_t; \hat{\theta}_k, \hat{\eta}^{(k)}) = 0$ (residual-on-residual OLS slope on block B_k). Under Assumptions 2.1, 2.3, 2.4, 2.5 and Lemma 2.1,

$$\sqrt{|B_k|}(\hat{\theta}_k - \theta_0) = A^{-1} \cdot \frac{1}{\sqrt{|B_k|}} \sum_{t \in B_k} \psi(W_t; \theta_0, \eta_0) + o_p(1), \quad k = 1, \dots, K,$$

where $A = \mathbb{E}[\partial_\theta \psi(W_t; \theta_0, \eta_0)]$ is nonsingular.

THEOREM 2.1. (FOLD-AVERAGE RCF ATTAINS ORACLE ASYMPTOTIC VARIANCE) Let $\hat{\theta} = K^{-1} \sum_{k=1}^K \hat{\theta}_k$ with $\hat{\theta}_k$ as above. Under Assumptions 2.1–2.5 and the invariance principle (Assumption 2.2),

$$\sqrt{T}(\hat{\theta} - \theta_0) \Rightarrow \mathcal{N}(0, V), \quad V := A^{-1} \Sigma A^{-1},$$

where Σ is the long-run variance in (2.6).

Although the main blocks B_1, \dots, B_K are disjoint, serial dependence in $\{W_t\}$ and overlapping auxiliary samples induce cross-fold covariance. The fold-specific estimators

$$\hat{\theta}_k \approx \theta_0 + A^{-1} \frac{1}{|B_k|} \sum_{t \in B_k} \psi(W_t; \theta_0, \eta_0),$$

are not independent across k , thus their average $\hat{\theta} = K^{-1} \sum_{k=1}^K \hat{\theta}_k$, accumulates these dependencies into the long-run variance which determines the asymptotic covariance of $\hat{\theta}$. Consequently, valid inference requires estimating Σ in a way that captures cross-fold serial dependence. We do this via an HAC estimator built from the stacked, time-ordered, cross-fitted score series $\{\hat{s}_t\}_{t=1}^T$ rather than by averaging per-fold variances. A full description of the variance estimator appears in the supplementary appendix.

3. STABILITY-BASED TUNING OF NUISANCE PARAMETERS

The validity of DML relies on Neyman orthogonality, which requires the second-stage score to be locally insensitive to small errors in nuisance estimation (Chernozhukov et al., 2018). This robustness holds only when nuisance learners satisfy the appropriate complexity conditions. Conditions, equivalently, when they achieve suitable L_2 -consistency.

In high-dimensional settings, tuning hyperparameters solely for predictive accuracy may violate these requirements. As shown by McGrath et al. (2025), prediction-optimal tuning can lead to nuisance estimates that undermine valid inference, even in cross-sectional designs. In practice, nuisance models cannot be too simple (leaving residual confounding) or too complex (absorbing treatment variation or overfitting noise).

This balance is often described as the Goldilocks zone of model complexity (Fort and Scherlis, 2019; Snyder et al., 2024), where $\hat{m}_0(X_t)$ removes confounding while preserving sufficient policy variation for identification, and $\hat{g}_0^T(X_t)$ denoises without attenuating policy-induced signals.

We operationalize this idea by targeting regions of the hyperparameter space that balance predictive accuracy and local stability, rather than selecting the hyperparameter that minimizes predictive error. Choosing within these stability regions avoids overfitting to sharp local minima and yields nuisance estimates that support more reliable second-stage inference. We therefore refer to our tuning method as identifying the Goldilocks zone of the time-series DML estimator.

Let $\Lambda = \{\lambda_1, \lambda_2, \dots, \lambda_M\}$ denote an ordered, equally spaced, grid of scalar hyperparameters (e.g., Lasso regularization penalties), sorted such that $\lambda_i < \lambda_{i+1}$. For a given fold k , let $\hat{\eta}^{(k)}(\lambda_i)$ be the nuisance function estimated on the auxiliary sample using parameter λ_i . Let $\mathcal{R}(\lambda_i)$ denote the RMSE of this estimate evaluated on the main block B_k . We consider a moving window of size S consisting of adjacent hyperparameters. For the j -th window, denoted as \mathcal{W}_j , the set of indices is defined as $\{j, j+1, \dots, j+S-1\}$ for $j = 1, \dots, M-S+1$.

For each window \mathcal{W}_j , we compute two component metrics: local variability and local predictive performance. Local variability is defined as

$$V_j = \frac{1}{S} \sum_{i \in \mathcal{W}_j} (\mathcal{R}(\lambda_i) - \bar{\mathcal{R}}_j)^2, \quad \text{where } \bar{\mathcal{R}}_j = \frac{1}{S} \sum_{i \in \mathcal{W}_j} \mathcal{R}(\lambda_i). \quad (3.9)$$

Intuitively, the local performance metric in each window will be given by $\bar{\mathcal{R}}_j$.

To ensure commensurability between stability and performance, we apply min-max normalizations $\tilde{V}_j = (V_j - \min V_j) / (\max V_j - \min V_j)$ and $\tilde{\mathcal{R}}_j = (\bar{\mathcal{R}}_j - \min \bar{\mathcal{R}}_j) / (\max \bar{\mathcal{R}}_j - \min \bar{\mathcal{R}}_j)$ across all valid windows j .

Each score \mathcal{S}_j then combines the normalized metrics:

$$\mathcal{S}_j = \tilde{V}_j + \tilde{\mathcal{R}}_j. \quad (3.10)$$

The Goldilocks zone, \mathcal{W}^* , is the window associated with the minimum score, balancing low predictive error with structural stability:

$$\mathcal{W}^* = \min_j \mathcal{S}_j. \quad (3.11)$$

Finally, the optimal hyperparameter λ^* is the minimizer of the predictive error within the Goldilocks zone:

$$\lambda^* = \arg \min_{\lambda_i \in \mathcal{W}^*} \mathcal{R}(\lambda_i). \quad (3.12)$$

This rule ensures that the chosen regularization parameter attains high predictive performance while lying in a region robust to small perturbations. In our implementation, we set the window size to $S = 3$.

4. SIMULATIONS

In this section, we present simulation evidence on the performance of RCF-DML using a contemporaneously recursive SVAR. The data-generating process (DGP) is given by

$$Y_t = \mu + \Phi_1 Y_{t-1} + \varepsilon_t, \quad \varepsilon_t = P u_t, \quad u_t \sim \mathcal{N}(0, I_n), \quad (4.13)$$

where $Y_t \in \mathbb{R}^n$ and P is a lower-triangular Cholesky factor encoding contemporaneous impacts. The autoregressive matrix Φ_1 induces approximate sparse local dependence via asymmetric, band-limited decay. We consider $p = 100$ covariance stationary variables and conduct 10,000 Monte Carlo simulations. Details on this and alternative DGPs are provided in Supplement S1.

Large sample, low complexity. We first evaluate the large-sample performance of the RCF-DML estimator by fixing the sample size at $T = 1,000$, which provides an approximation to the asymptotic regime. We use RMSE-tinned Lasso for nuisances' approximations.⁹

The results in Table 1 show that the RCF-DML estimator attains nominal coverage and exhibits asymptotic consistency, with percentage bias remaining close to 1.5%. The correct coverage and small bias indicate that the FCLT operates as expected, yielding asymptotic normality. Moreover, the estimator performance is stable across the range of fold choices. Taken together, these findings confirm the analytical properties established for the RCF-DML procedure and, importantly, validate the HAC variance estimation strategy adopted in the asymptotic analysis.

Table 1: Simulation results for bias and 95% coverage (Asymptotic).

	K=4	K=5	K=6	K=7	K=8	K=9	K=10	K=11	K=12
Bias	1.5	1.6	1.7	1.7	1.6	1.5	1.6	1.6	1.6
Coverage	94.1	94.0	94.1	94.3	94.1	94.4	93.9	94.3	93.6

Note: Bias and 95% coverage across horizons (K) for sample size $T = 1000$. Results are obtained over 10,000 Monte Carlo replications.

Small samples, high complexity. We next document the bias-reduction gains achieved by the Goldilocks zone (GZ) tuning rule in finite samples relative to the standard predictive metric (RMSE), and compare the performance of the RCF-DML estimator with the alternative NLO cross-fitting strategy. We consider sample sizes $T \in \{50, 100, 200\}$ and different values of K . Using the complexity measure $c = p/T$ (McGrath et al. 2025), this design spans a range of dimensionality regimes, from high-dimensional settings ($c = 2$ and $c = 1$) to moderately complex ones ($c = 0.5$).

The results depicted in Table 2 show clear bias-reduction benefits of the stability-based tuning rule (RCF-GZ), particularly in small samples where high dimensionality amplifies overfitting risk. In these settings, on average, the RCF-GZ reduces bias by approximately 35% relative to RCF-RMSE. In addition, the bias decreases with larger values of K under

⁹Because the SVAR design is low-complexity relative to the sample size, tuning the Lasso penalty via the Goldilocks zone offers no improvement, such that the optimal parameter λ^* is selected using the standard predictive criterion.

both tuning methods, though GZ consistently yields the more substantial improvement. The estimator's coverage is largely insensitive to the choice of the tuning metric. Coverage remains close to the nominal rate under both the GZ and RMSE criteria, and displays substantial stability across different values of K .

Table 2: Simulation results for bias and 95% coverage (Finite Sample).

K	T = 50						T = 100						T = 200					
	RCF-GZ		RCF-RMSE		NLO-RMSE		RCF-GZ		RCF-RMSE		NLO-RMSE		RCF-GZ		RCF-RMSE		NLO-RMSE	
	Bias	Cov	Bias	Cov	Bias	Cov	Bias	Cov	Bias	Cov	Bias	Cov	Bias	Cov	Bias	Cov	Bias	Cov
4	6.2	88.8	7.6	88.5	10.5	81.1	3.7	91.0	4.3	91.0	8.3	86.6	2.1	93.2	2.8	92.9	5.4	89.3
5	5.3	88.5	6.6	88.0	9.4	80.0	3.3	91.2	4.3	90.8	6.6	86.7	1.5	93.0	2.4	92.5	3.8	90.1
6	5.6	87.9	7.3	87.4	8.7	75.9	3.2	90.7	4.3	90.1	5.4	85.4	2.3	93.2	3.2	92.7	3.7	90.2
7	5.2	86.8	7.1	86.4	8.2	73.1	3.4	91.1	4.7	90.7	5.5	85.2	1.7	93.1	2.7	92.8	3.1	90.3
8	5.3	86.4	7.3	85.9	7.6	69.4	3.1	90.1	4.5	89.5	4.6	83.5	1.4	92.6	2.5	91.8	2.5	90.1
9	4.9	86.1	6.8	85.7	7.7	64.2	2.7	89.6	4.2	88.9	4.5	82.5	1.4	92.3	2.5	91.9	2.5	89.6
10	4.1	86.9	6.0	85.9	6.7	64.3	2.7	89.6	4.3	88.9	3.8	81.2	1.4	92.0	2.6	91.8	2.2	88.9
11	4.6	85.1	7.4	84.2	7.6	60.8	2.1	89.5	3.7	89.1	3.4	79.6	1.1	92.2	2.4	91.6	2.1	88.3
12	3.6	85.7	6.1	84.7	6.0	62.0	2.8	89.4	4.3	88.6	3.8	77.9	1.2	91.8	2.5	91.4	2.0	88.0

Note: Bias and 95% coverage across horizons (K) and sample sizes (T). Results are obtained over 10,000 Monte Carlo replications.

Relative to the NLO CF estimator (NLO-RMSE), RCF-RMSE reduces bias by about 10% on average, with larger gains in smaller samples. RCF-GZ delivers over a 40% reduction. Even for $K \geq 10$, when NLO-RMSE remains root- T consistent, the bias under NLO-RMSE is still more than 35% higher than under RCF-GZ. To further demonstrate that the GZ metric is not specific to our CF strategy, the supplementary appendix reports parallel simulations using the NLO-GZ procedure. Even under that CF design, the proposed metric improves the estimator's accuracy relative to standard RMSE-based tuning, without compromising coverage.¹⁰

Overall, the results show that RCF can improve on NLO in small samples with high serial dependence. In such cases, the trade-off between sample usage and near-independence becomes binding: for NLO, increasing K leaves too little data in each left-out block to satisfy the independence condition. As expected, these issues diminish as T grows.

Violating the normality assumption: GARCH heteroskedasticity We consider the case in which the time-reversibility condition is violated by introducing GARCH heteroskedasticity. The specific GARCH structure is detailed, together with simulation results, in the supplementary appendix.

Compared with the homoskedastic benchmark, both RCF and NLO-DML exhibit higher bias. However, RCF-DML coverage remains close to its nominal rate. Notably, the RCF-DML estimator remains approximately root- T consistent across different values of K . Compared with the time-directional NLO design, the gains from increased sample usage and estimator efficiency under RCF outweigh the losses induced by heteroskedasticity and non-invertibility. Overall, deviations from homoskedasticity moderately affect the accuracy of the time-series DML estimator but do not impair its inferential properties.

Double Machine Learning for Local Projections. We show that the RCF-DML methodology can be used to estimate dynamic causal effects. In this case, the ground-truth

¹⁰Although the NLO design aims to produce approximately independent folds, we estimate its standard errors using the same HAC procedure as for RCF-DML to account for possible residual serial dependence.

target is the recursive solution of the SVAR. The IRF of the outcome variable to the shock of interest is estimated using the LP adaptation¹¹ of the DML-PLR model defined in equations 1.1 and 1.2, namely:

$$y_{t+h} = \theta_h d_t + g_h(X_t) + \epsilon_{t+h}, \quad E[\epsilon_{t+h} | X_t, d_t] = 0, \quad (4.14)$$

$$d_t = m_0(X_t) + \xi_t, \quad E[\xi_t | X_t] = 0, \quad (4.15)$$

for horizons $h = 0, 1, \dots, H$.

The DML-LP implementation requires re-estimating, for every horizon, the fold-specific nuisance functions of the reduced-form outcome equation. The resulting dynamic residualized equation is:

$$\hat{\chi}_{t+h} = \theta_h \hat{\xi}_t + \epsilon_{t+h} \quad (4.16)$$

where $\hat{\chi}_{t+h} = y_{t+h} - \hat{g}_h^r(X_t)$, $\hat{\xi}_t = d_t - \hat{m}_0(X_t)$, and $\hat{g}_h^r \neq g_h$ denotes the reduced-form mapping for the outcome equation employed in the residualization step.

The finite sample properties of the RCF-DML-LP estimator, considering eight horizons, are reported in the supplementary appendix. The bias remains very small and converges to zero at longer horizons, where the true IRF decays. Coverage remains close to its nominal level, including the high-dimensional regime with the smallest sample size.

5. APPLICATION

We apply the time-series RCF-DML LP estimator developed above to assess the dynamic effects of prudential capital shocks on Italian GDP, private nonfinancial corporations (PNFC) lending, PNFC spreads, and the components of the Tier 1 capital ratio. Because prudential tools were introduced only recently, the available time series are short. This data feature makes the RCF approach suitable for inference in this setting.

Since its introduction in 1988, the Basel I framework has established minimum capital requirements to strengthen banking system stability and laid the foundation for subsequent Basel Accords. In the aftermath of the 2008 financial crisis, financial institutions exhibited significant fragility (cited in Admati and Hellwig, 2014), leading regulators to reach consensus on the need to strengthen bank capital and liquidity requirements. The Basel Committee on Banking Supervision (BCBS) introduced a broad set of reforms on September 12, 2010, aimed at enhancing the resilience of the global financial system (BCBS, 2010a). The Basel framework is expected to curb banks' risk-taking incentives (Holmstrom and Tirole, 1997; Kim and Santomero, 1988) and lower default probabilities following adverse shocks (Dewatripont and Tirole, 1994; Gambacorta and Mistrulli, 2004). However, policymakers and industry participants have raised concerns that these regulations may entail sizable costs for banks and the real economy (Fédération Bancaire Française (FBF), 2010; Institute of International Finance (IIF), 2011).

A growing empirical literature evaluates the macroeconomic consequences of bank capital shocks. Empirical studies, using various identification schemes and alternative capital measures, largely converge on the same conclusions: prudential capital shocks reduce economic activity in the short run, contract corporate lending, and increase lending spreads. Table 3 summarizes the main dynamic estimates of the effects of prudential capital shocks on GDP, PNFC lending, and interest-rate spreads from leading empirical contributions.

¹¹Chernozhukov et al. (2021) and Agostini et al. (2024) provide early applications of DML to LP settings.

Table 3. The impact of bank capital shocks: a comparison (All effects are scaled to a 50 basis points increase in the primary capital metric used to transmit the shock).

Reference	Country	Evaluation after...	Real GDP (%)	PNFC lending (%)	PNFC spread (bps)
Noss and Toffano (2016)	UK	2 quarters	-0.3 ^a	-1.0	N/A
Meeks (2017)	UK	6 quarters	-0.1	-1.3	2
Mésonnier and Stevanovic (2017)	US	4 quarters	-0.7	-3.0	30 ^b
Kanngiesser et al. (2020)	EA	on impact	-0.6	-1.2 ^c	10
Conti et al. (2023)	Italy	2 quarters	-0.1	-0.12	3

Note: ^a Denotes not significant estimate; ^b Impact after 2 quarters; ^c Impact after 4 quarters; The panel of the table compares IRF results across studies. The primary capital metrics used to transmit the shock in each paper are as follows: Noss and Toffano (2016) use the capital-to-asset ratio; Meeks (2017) uses the trigger ratio; Mésonnier and Stevanovic (2017), Kanngiesser et al. (2020) use the capital buffer; Conti et al. (2023) use Tier 1 / RWA.

5.1. Data and Methodology

We construct our dataset using official sources and following several related studies (Conti et al., 2023; Kanngiesser et al., 2020; Meeks, 2017; Mésonnier and Stevanovic, 2017; Noss and Toffano, 2016). These works guide the identification of variables that act as transmission channels through which capital requirements influence banks' capital ratios and the broader economy.

We consider an extensive set of controls to isolate the causal effect of regulatory capital on GDP.¹² To avoid conditioning on post-treatment mediators, which would block part of the causal transmission mechanism (Pearl, 2009), transmission-channel variables enter the model only lagged.¹³ The policy variable is the Tier 1 Capital to Risk-Weighted Assets, sourced from the IMF.¹⁴ We test each outcome, the policy, and control series for stationarity and apply log-differences to variables in levels and differences to ratios and interest rates.¹⁵

The dynamic analysis considers the DML-LP model defined by equations 4.14, 4.15, and 4.16 together with the residualized regression in equation 4.16. We approximate the nuisance functions using Lasso. We fix the number of folds to $K = 8$,¹⁶ and tune the fold-specific shrinkage intensity parameters according to the Goldilocks zone target over a grid of 10.000 values. The predictive equations and residuals are fitted on the auxiliary sample and evaluated on the main sample. In practice, the orthogonalized residuals are computed using the "Best" estimator among all candidates within the Goldilocks zone.

We focus on four main channels through which prudential capital shocks affect real GDP. These are Tier 1 capital, risk-weighted assets of Italian banks, the real value of banks' new loans to PNFCs, and the PNFC interest-rate spread, computed as the difference between the lending rate on new loans and the three-month Euribor (Conti et al., 2023).

¹²We provide in the supplementary appendix the lists of all variables used and their sources.

¹³We include three lags of the control variables, the outcome, and the policy variable.

¹⁴<https://data.imf.org/?sk=51B096FA-2CD2-40C2-8D09-0699CC1764DA>. The IMF reports half-quarterly data for Italy from 2005Q2. To construct a consistent quarterly series, we interpolate the IMF data. Validation exercises confirm that the interpolation preserves the structure of the underlying data.

¹⁵All series are seasonally adjusted using X-13ARIMA-SEATS (Monsell, 2007).

¹⁶With eight CF folds, and considering $H = 8$, we maximize sample usage.

5.2. Results

The shock leads to an increase in the PNFC spread, peaking at about three basis points after three quarters. In turn, the reduction in corporate lending, which carries relatively higher regulatory risk weights, is consistent with banks prioritizing the downsizing of higher risk-weighted assets to meet tighter capital-ratio requirements.

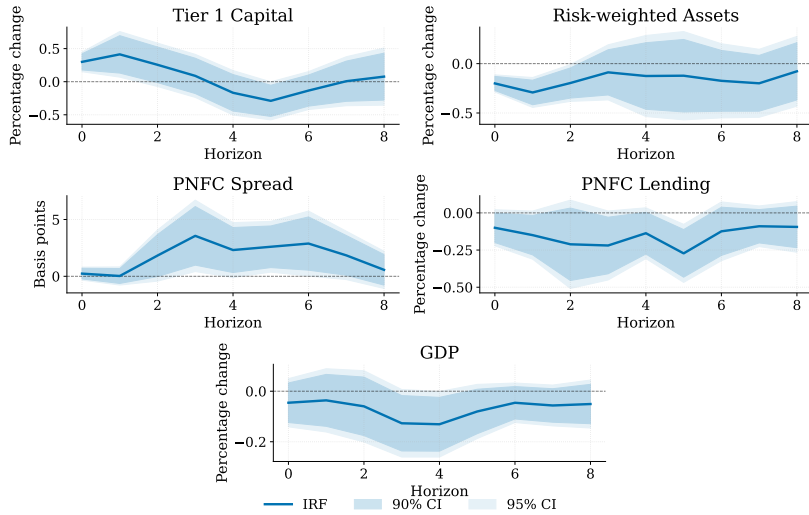


Figure 2. Cumulative Impulse response functions to a regulatory capital shock obtained via RCF-DML LPs. The dark (light) blue shaded areas denote 95% (90%) cumulative confidence intervals computed via HAC.

A reduction in credit supply generates adverse short-run macroeconomic effects that gradually fade in the medium term. Real GDP contracts by almost 0.13 percent after four quarters.

The method successfully recovers the expected transmission patterns of prudential capital shocks and aligns closely with established empirical evidence summarized in Table 3. The supplementary appendix reports the corresponding impulse responses obtained using the RMSE-based calibration of the nuisance functions.

These results further highlight the validity of the novel metric proposed in this paper, particularly for addressing the real GDP response. For the latter, RMSE tuning tends to over-denoise the series and attenuate the policy signal, leading to a non-significant response, contrasting with the existing literature.

6. CONCLUSIONS

This paper develops a Double Machine Learning estimator for macroeconomic time series, where short samples, persistence, and endogeneity limit the effectiveness of standard cross-fitting and predictive tuning.

We contribute two methodological innovations. First, Reverse Cross-Fitting, exploiting the time-reversibility of stationary processes to construct folds that increase sample usage

while preserving the asymptotic independence conditions for orthogonal scores. Second, the Goldilocks zone tuning rule is a stability-based criterion that targets hyperparameter regions that jointly deliver predictive performance and local stability. Together, these features improve estimation accuracy in short and dependent samples while maintaining the formal inferential guarantees of Double Machine Learning.

We prove that the estimator admits an asymptotic linear representation, is \sqrt{T} -consistent and asymptotically normal, and that HAC estimators consistently recover the long-run variance.

Monte Carlo experiments confirm these theoretical results. In approximately sparse time-series designs, the estimator with Reverse Cross-Fitting yields lower bias and more stable coverage than existing cross-fitting schemes, particularly in short samples with strong dependence. The Goldilocks tuning rule further improves accuracy and enhances the performance of other cross-fitted DML variants. Deviations from time-reversibility, such as GARCH volatility, reduce accuracy but do not undermine inferential validity.

We also extend the framework to dynamic causal analysis using Local Projections with DML residualization. The results display limited bias and correct coverage under the model, even under high-dimensional controls.

An empirical application to prudential capital shocks in Italy illustrates the method's practical relevance. The DML estimator with Reverse Cross-Fitting yields economically plausible impulse responses aligned with established evidence.

Our approach offers an alternative, rather than a universally superior, adaptation of Double Machine Learning to serially dependent data. Theoretical and simulation results characterize the settings in which Reverse Cross-Fitting is most advantageous.

Overall, the paper provides a feasible and theoretically grounded framework for deploying orthogonal-score methods in macroeconomic time series, a context in which standard DML is unreliable and structural uncertainty is substantial.

REFERENCES

- Adamek, R., Smeeke, S., and Wilms, I. (2024). Local projection inference in high dimensions. *The Econometrics Journal*, 27(3), 323–342.
- Admati, A. and Hellwig, M. (2014). *The bankers' new clothes: What's wrong with banking and what to do about it*. Princeton University Press.
- Agostini, E., Bloise, F., and Tancioni, M. (2024). Vaccination policy and mortality from COVID-19 in the European Union. *The Econometrics Journal*, 27(2), 299–322.
- Ahrens, A., Chernozhukov, V., Hansen, C., Kozbur, D., Schaffer, M., and Wiemann, T. (2025). An introduction to double/debiased machine learning. arXiv preprint arXiv:2504.08324.
- Ahrens, A., Hansen, C. B., Schaffer, M. E., and Wiemann, T. (2025). Model Averaging and Double Machine Learning. *Journal of Applied Econometrics*, 40, 249–269.
- Andrews, D. W. K. (1991). Heteroskedasticity and autocorrelation consistent covariance matrix estimation. *Econometrica*, 59(3), 817–858.
- Athey, S. and Imbens, G. (2016). Recursive partitioning for heterogeneous causal effects. *Proceedings of the National Academy of Sciences*, 113(27), 7353–7360.
- Athey, S. and Wager, S. (2019). Estimating treatment effects with causal forests: An application. *Observational Studies*, 5(2), 37–51.
- Athey, S., Tibshirani, J., and Wager, S. (2019). Generalized random forests.
- BCBS (2010a). An assessment of the long-term economic impact of stronger capital and liquidity requirements. *Basel Committee on Banking Supervision*.

- Belloni, A., Chernozhukov, V., and Hansen, C. (2014). High-dimensional methods and inference on structural and treatment effects. *Journal of Economic Perspectives*, 28(2), 29–50.
- Billingsley, P. (1968). *Convergence of Probability Measures*. New York: John Wiley & Sons.
- Celentano, M. and Wainwright, M. J. (2023). Challenges of the inconsistency regime: Novel debiasing methods for missing data models. arXiv preprint arXiv:2309.01362.
- Chang, N.-C. (2020). Double/debiased machine learning for difference-in-differences models. *The Econometrics Journal*, 23(2), 177–191.
- Cheng, Q. (1999). Miscellanea. On time-reversibility of linear processes. *Biometrika*, 86(2), 483–486.
- Chernozhukov, V., Chetverikov, D., Demirer, M., Duflo, E., Hansen, C., Newey, W., and Robins, J. (2018). Double/debiased machine learning for treatment and structural parameters. *The Econometrics Journal*, 21(1), C1–C68.
- Chernozhukov, V., Kasahara, H., and Schrimpf, P. (2021). Causal impact of masks, policies, behavior on early covid-19 pandemic in the US. *Journal of Econometrics*, 220(1), 23–62.
- Chernozhukov, V., Escanciano, J. C., Ichimura, H., Newey, W. K., and Robins, J. M. (2022a). Locally Robust Semiparametric Estimation. *Econometrica*, 90(4), 1501–1535.
- Chernozhukov, V., Newey, W. K., and Singh, R. (2022b). Automatic Debiased Machine Learning of Causal and Structural Effects. *Econometrica*, 90(3), 967–1027.
- Conti, A. M., Nobili, A., and Signoretti, F. M. (2023). Bank capital requirement shocks: A narrative perspective. *European Economic Review*, 151, 104254.
- Dewatripont, M. and Tirole, J. (1994). A theory of debt and equity: Diversity of securities and manager-shareholder congruence. *The Quarterly Journal of Economics*, 109(4), 1027–1054.
- Dube, A., Jacobs, J., Naidu, S., and Suri, S. (2020). Monopsony in online labor markets. *American Economic Review: Insights*, 2(1), 33–46.
- Fédération Bancaire Française (FBF) (2010). Reforming of Prudential Rules: Position of French Banks With Regard To Current Proposals. Working Paper, Fédération Bancaire Française, Paris.
- Fort, S. and Scherlis, A. (2019). The goldilocks zone: Towards better understanding of neural network loss landscapes. In *Proceedings of the AAAI Conference on Artificial Intelligence*, Volume 33, pp. 3574–3581.
- Gambacorta, L. and Mistrulli, P. E. (2004). Does bank capital affect lending behavior? *Journal of Financial Intermediation*, 13(4), 436–457.
- Giannone, D., Lenza, M., and Primiceri, G. E. (2021). Economic predictions with big data: The illusion of sparsity. *Econometrica*, 89(5), 2409–2437.
- Hallin, M., Lefevre, C., and Puri, M. L. (1988). On time-reversibility and the uniqueness of moving average representations for non-Gaussian stationary time series. *Biometrika*, 75(1), 170–171.
- Hansen, L. P. (1982). Large sample properties of generalized method of moments estimators. *Econometrica*, 50(4), 1029–1054.
- Herrndorf, N. (1984). A functional central limit theorem for strongly mixing sequences of random variables. *Annals of Probability*, 12(1), 141–153.
- Holmstrom, B. and Tirole, J. (1997). Financial intermediation, loanable funds, and the real sector. *The Quarterly Journal of Economics*, 112(3), 663–691.

- Institute of International Finance (IIF) (2011). The Cumulative Impact on the Global Economy of Proposed Changes in the Banking Regulatory Framework. Final Report, Institute of International Finance, Washington, D.C.
- Jaeger, D. A. (1995). Problems with instrumental variables estimation when the correlation between the instruments and the endogenous explanatory variable is weak. *Journal of the American Statistical Association*.
- Kanngiesser, D., Martin, R., Maurin, L., and Moccerro, D. (2020). The macroeconomic impact of shocks to bank capital buffers in the Euro Area. *The BE Journal of Macroeconomics*, 20(1), 20180009.
- Kim, D. and Santomero, A. M. (1988). Risk in banking and capital regulation. *The Journal of Finance*, 43(5), 1219–1233.
- Martínez, J. H., Herrera-Diestra, J. L., and Chavez, M. (2018). Detection of time reversibility in time series by ordinal patterns analysis. *Chaos: An Interdisciplinary Journal of Nonlinear Science*, 28(12), 123111.
- Maxwell, M., and Woodroffe, M. (2000). Central limit theorems for additive functionals of Markov chains. *Annals of Probability*, 28(2), 713–724.
- McClellan, A., Balakrishnan, S., Kennedy, E. H., and Wasserman, L. (2024). Double cross-fit doubly robust estimators: Beyond series regression. arXiv preprint arXiv:2403.15175.
- McGrath, S., Mukherjee, D., Mukherjee, R., and Wang, Z. J. (2025). Optimal Nuisance Function Tuning for Estimating a Doubly Robust Functional under Proportional Asymptotics. arXiv preprint arXiv:2509.25536.
- Meeks, R. (2017). Capital regulation and the macroeconomy: Empirical evidence and macroprudential policy. *European Economic Review*, 95, 125–141.
- Mésonnier, J.-S. and Stevanovic, D. (2017). The macroeconomic effects of shocks to large banks' capital. *Oxford Bulletin of Economics and Statistics*, 79(4), 546–569.
- Monsell, B. C. (2007). The X-13A-S seasonal adjustment program. In *Proceedings of the 2007 Federal Committee On Statistical Methodology Research Conference*, pp. 515.
- Noss, J. and Toffano, P. (2016). Estimating the impact of changes in aggregate bank capital requirements on lending and growth during an upswing. *Journal of Banking & Finance*, 62, 15–27.
- Pearl, J. (2009). Causal inference in statistics: An overview. *Statistics Surveys*, 3, 96–146.
- Robinson, P. M. (1988). Root-N-consistent semiparametric regression. *Econometrica: Journal of the Econometric Society*, 931–954.
- Rothman, P. A. (1990). *Characterization of the time irreversibility of economic time series*. New York University.
- Semenova, V. and Chernozhukov, V. (2021). Debiased machine learning of conditional average treatment effects and other causal functions. *The Econometrics Journal*, 24(2), 264–289.
- Semenova, V., Goldman, M., Chernozhukov, V., and Taddy, M. (2023). Inference on heterogeneous treatment effects in high-dimensional dynamic panels under weak dependence. *Quantitative Economics*, 14(2), 471–510.
- Snyder, S. H., Vignaux, P. A., Ozalp, M. K., Gerlach, J., Puhl, A. C., Lane, T. R., Corbett, J., Urbina, F., and Ekins, S. (2024). The Goldilocks paradigm: comparing classical machine learning, large language models, and few-shot learning for drug discovery applications. *Communications Chemistry*, 7(1), 134.
- Tong, H. and Zhang, Z. (2005). On time-reversibility of multivariate linear processes. *Statistica Sinica*, 495–504.
- Weiss, G. (1975). Time-reversibility of linear stochastic processes. *Journal of Applied Probability*, 12(4), 831–836.

APPENDIX A: PROOFS OF RESULTS

Proof of LEMMA 2.1

PROOF. Throughout, $|B_k| \asymp T$ because K is fixed; all $o_p(\cdot)$ rates are uniform in k .

Step 1 (Orthogonal expansion with L_2 -quadratic remainder). By Assumption 2.3, for each $t \in B_k$,

$$\psi(W_t; \theta_0, \hat{\eta}^{(k)}) - \psi(W_t; \theta_0, \eta_0) = \underbrace{\partial_\eta \psi(W_t; \theta_0, \eta_0) [\Delta^{(k)}]}_{=: L_t^{(k)}} + r_t^{(k)}, \quad \Delta^{(k)} := \hat{\eta}^{(k)} - \eta_0, \quad (\text{A.1})$$

with $\mathbb{E}[(r_t^{(k)})^2] \lesssim \|\Delta^{(k)}\|_{L_2}^4$. By Neyman orthogonality in Assumption 2.3,

$$\mathbb{E}[L_t^{(k)}] = \mathbb{E}[\partial_\eta \psi(W_t; \theta_0, \eta_0) [\Delta^{(k)}]] = 0 \quad (\text{unconditional}). \quad (\text{A.2})$$

Step 2 (Decomposition into conditional mean and centered part). Define the conditional means

$$\bar{L}_t^{(k)} := \mathbb{E}[L_t^{(k)} \mid \mathcal{F}_{\text{aux},k}], \quad \bar{r}_t^{(k)} := \mathbb{E}[r_t^{(k)} \mid \mathcal{F}_{\text{aux},k}].$$

Average (A.1) over $t \in B_k$ and add/subtract the conditional means:

$$R_k = \underbrace{\frac{1}{|B_k|} \sum_{t \in B_k} (\bar{L}_t^{(k)} + \bar{r}_t^{(k)})}_{(\text{A}) \text{ conditional mean}} + \underbrace{\frac{1}{|B_k|} \sum_{t \in B_k} [(L_t^{(k)} - \bar{L}_t^{(k)}) + (r_t^{(k)} - \bar{r}_t^{(k)})]}_{(\text{B}) \text{ centered fluctuation}}.$$

We will show: (A) = $o_p(T^{-1/2})$ and (B) = $o_p(T^{-1/2})$.

Step 2.1 (Term A is small). Assumption 2.4 (conditional stability) gives directly

$$\left\| \mathbb{E} \left[\frac{1}{|B_k|} \sum_{t \in B_k} \{ \psi(W_t; \theta_0, \hat{\eta}^{(k)}) - \psi(W_t; \theta_0, \eta_0) \} \mid \mathcal{F}_{\text{aux},k} \right] \right\| = o_p(T^{-1/2}),$$

which equals $\left\| \frac{1}{|B_k|} \sum_{t \in B_k} (\bar{L}_t^{(k)} + \bar{r}_t^{(k)}) \right\|$ by (A.1). Hence (A) = $o_p(T^{-1/2})$.

Step 2.2 (Term B). Condition on $\mathcal{F}_{\text{aux},k}$ so that $\Delta^{(k)}$ is fixed. For the linear part,

$$L_t^{(k)} - \bar{L}_t^{(k)} = \left(\partial_\eta \psi(W_t; \theta_0, \eta_0) - \mathbb{E}[\partial_\eta \psi(W_t; \theta_0, \eta_0) \mid \mathcal{F}_{\text{aux},k}] \right) [\Delta^{(k)}].$$

Thus,

$$\begin{aligned} & \mathbb{E} \left[\left\| \frac{1}{|B_k|} \sum_{t \in B_k} (L_t^{(k)} - \bar{L}_t^{(k)}) \right\|^2 \mid \mathcal{F}_{\text{aux},k} \right] \\ &= \frac{1}{|B_k|^2} \sum_{t,s \in B_k} \mathbb{E} \left[\left\langle (\mathcal{G}_t - \bar{\mathcal{G}}) [\Delta^{(k)}], (\mathcal{G}_s - \bar{\mathcal{G}}) [\Delta^{(k)}] \right\rangle \mid \mathcal{F}_{\text{aux},k} \right], \quad (\text{A.3}) \end{aligned}$$

where we set $\mathcal{G}_t := \partial_\eta \psi(W_t; \theta_0, \eta_0)$ and $\bar{\mathcal{G}} := \mathbb{E}[\mathcal{G}_t \mid \mathcal{F}_{\text{aux},k}]$ for brevity, and $\langle \cdot, \cdot \rangle$ denotes the Euclidean inner product in \mathbb{R}^d .

By Cauchy-Schwarz and operator norms,

$$|\langle (\mathcal{G}_t - \bar{\mathcal{G}})[\Delta], (\mathcal{G}_s - \bar{\mathcal{G}})[\Delta] \rangle| \leq \|\Delta\|^2 \|\mathcal{G}_t - \bar{\mathcal{G}}\|_{\text{op}} \|\mathcal{G}_s - \bar{\mathcal{G}}\|_{\text{op}}.$$

Taking conditional expectations and summing by lags $h = t - s$,

$$\begin{aligned} & \mathbb{E} \left[\left\| \frac{1}{|B_k|} \sum_{t \in B_k} (L_t^{(k)} - \bar{L}_t^{(k)}) \right\|^2 \middle| \mathcal{F}_{\text{aux},k} \right] \\ & \leq \frac{\|\Delta^{(k)}\|^2}{|B_k|^2} \sum_{t,s \in B_k} \mathbb{E}[\|\mathcal{G}_t - \bar{\mathcal{G}}\|_{\text{op}} \|\mathcal{G}_s - \bar{\mathcal{G}}\|_{\text{op}} \mid \mathcal{F}_{\text{aux},k}] \\ & \lesssim \frac{\|\Delta^{(k)}\|^2}{|B_k|^2} \sum_{h=-(|B_k|-1)}^{|B_k|-1} (|B_k| - |h|) \Gamma_{\mathcal{G}}(h), \end{aligned} \quad (\text{A.4})$$

where $\Gamma_{\mathcal{G}}(h) := \mathbb{E}[\|\mathcal{G}_t - \mathbb{E}\mathcal{G}_t\|_{\text{op}} \|\mathcal{G}_{t-h} - \mathbb{E}\mathcal{G}_{t-h}\|_{\text{op}}]$ is the lag- h autocovariance of the operator norms. By Assumption 2.3(ii), $\sum_h \Gamma_{\mathcal{G}}(h) < \infty$, and the Cesàro weights $(|B_k| - |h|)/|B_k| \leq 1$ imply

$$\mathbb{E} \left[\left\| \frac{1}{|B_k|} \sum_{t \in B_k} (L_t^{(k)} - \bar{L}_t^{(k)}) \right\|^2 \middle| \mathcal{F}_{\text{aux},k} \right] \lesssim \frac{\|\Delta^{(k)}\|^2}{|B_k|} \sum_h \Gamma_{\mathcal{G}}(h) \lesssim \frac{\|\Delta^{(k)}\|^2}{|B_k|}. \quad (\text{A.5})$$

Taking square roots and using $\|\Delta^{(k)}\| = o_p(T^{-1/4})$ (Assumption 2.4) and $|B_k| \asymp T$,

$$\left\| \frac{1}{|B_k|} \sum_{t \in B_k} (L_t^{(k)} - \bar{L}_t^{(k)}) \right\| = O_p \left(\frac{\|\Delta^{(k)}\|}{\sqrt{|B_k|}} \right) = o_p(T^{-1/4} \cdot T^{-1/2}) = o_p(T^{-3/4}) \subset o_p(T^{-1/2}). \quad (\text{A.6})$$

Step 2.3 (Centered quadratic remainder). By conditional Jensen and Assumption 2.3,

$$\mathbb{E}[(\bar{r}_t^{(k)})^2 \mid \mathcal{F}_{\text{aux},k}] \leq \mathbb{E}[(r_t^{(k)})^2 \mid \mathcal{F}_{\text{aux},k}] \lesssim \|\Delta^{(k)}\|^4 = o_p(T^{-1}).$$

Hence, still conditionally on $\mathcal{F}_{\text{aux},k}$ and using the same short-memory argument as in (A.5),

$$\begin{aligned} & \mathbb{E} \left[\left\| \frac{1}{|B_k|} \sum_{t \in B_k} (r_t^{(k)} - \bar{r}_t^{(k)}) \right\|^2 \middle| \mathcal{F}_{\text{aux},k} \right] \lesssim \frac{1}{|B_k|} \mathbb{E}[(r_t^{(k)})^2 \mid \mathcal{F}_{\text{aux},k}] \\ & = \frac{1}{|B_k|} o_p(T^{-1}) = o_p(T^{-2}). \end{aligned} \quad (\text{A.7})$$

Taking square roots and using the law of iterated expectations,

$$\left\| \frac{1}{|B_k|} \sum_{t \in B_k} (r_t^{(k)} - \bar{r}_t^{(k)}) \right\| = o_p(T^{-1}) \subset o_p(T^{-1/2}). \quad (\text{A.8})$$

Step 2.4 (Term B conclusion). Combine (A.6) and (A.8):

$$\frac{1}{|B_k|} \sum_{t \in B_k} [(L_t^{(k)} - \bar{L}_t^{(k)}) + (r_t^{(k)} - \bar{r}_t^{(k)})] = o_p(T^{-1/2}),$$

uniformly in k . Together with Step 2.1, we conclude $R_k = o_p(T^{-1/2})$ uniformly in k .

Step 3 (Conclusion) Equation (2.7) follows immediately from (A.1) and $R_k = o_p(T^{-1/2})$. Averaging (2.7) over k gives (2.8) because K is fixed and the $o_p(T^{-1/2})$ term is uniform in k . \square

Proof of LEMMA 2.2

PROOF. Define

$$\hat{A}_k(\vartheta) := \frac{1}{|B_k|} \sum_{t \in B_k} \partial_\theta \psi(W_t; \vartheta, \hat{\eta}^{(k)}), \quad \hat{A}_k := \hat{A}_k(\theta_0), \quad A := \mathbb{E}[\partial_\theta \psi(W_t; \theta_0, \eta_0)].$$

Step 1 (Mean-value identity in θ). By Gateaux differentiability in θ (Assumption 2.3), there exists $\tilde{\theta}_k$ on the line segment between θ_0 and $\hat{\theta}_k$ such that

$$0 = \frac{1}{|B_k|} \sum_{t \in B_k} \psi(W_t; \theta_0, \hat{\eta}^{(k)}) + \hat{A}_k(\tilde{\theta}_k) (\hat{\theta}_k - \theta_0).$$

Hence

$$\hat{\theta}_k - \theta_0 = -\hat{A}_k(\tilde{\theta}_k)^{-1} \cdot \frac{1}{|B_k|} \sum_{t \in B_k} \psi(W_t; \theta_0, \hat{\eta}^{(k)}). \quad (\text{A.9})$$

Step 2 (Orthogonal plug-in reduction to the oracle score). By Lemma 2.1 (using Assumptions 2.3 and 2.4),

$$\frac{1}{|B_k|} \sum_{t \in B_k} \psi(W_t; \theta_0, \hat{\eta}^{(k)}) = \frac{1}{|B_k|} \sum_{t \in B_k} \psi(W_t; \theta_0, \eta_0) + o_p(|B_k|^{-1/2}),$$

uniformly in k (since K is fixed).

Step 3 (Stability of the per-fold Jacobian). We show $\hat{A}_k(\tilde{\theta}_k) \rightarrow_p A$, which implies invertibility with probability approaching 1 and $\hat{A}_k(\tilde{\theta}_k)^{-1} \rightarrow_p A^{-1}$. Decompose

$$\begin{aligned} \hat{A}_k(\tilde{\theta}_k) - A &= \underbrace{\frac{1}{|B_k|} \sum_{t \in B_k} \{\partial_\theta \psi(W_t; \tilde{\theta}_k, \eta_0) - \partial_\theta \psi(W_t; \theta_0, \eta_0)\}}_{(I)} \\ &\quad + \underbrace{\frac{1}{|B_k|} \sum_{t \in B_k} \{\partial_\theta \psi(W_t; \tilde{\theta}_k, \hat{\eta}^{(k)}) - \partial_\theta \psi(W_t; \tilde{\theta}_k, \eta_0)\}}_{(II)} \\ &\quad + \underbrace{\frac{1}{|B_k|} \sum_{t \in B_k} \{\partial_\theta \psi(W_t; \theta_0, \eta_0) - A\}}_{(III)}. \end{aligned}$$

For (III), by Assumption 2.3(ii) (derivative stationarity with summable autocovariances), a law of large numbers applies, hence (III) = $o_p(1)$. For (II), by Assumption 2.3(iii) (Lipschitz in η in L_2) and the rate $\|\hat{\eta}^{(k)} - \eta_0\|_{L_2} = o_p(1)$ (Assumption 2.4), (II) = $o_p(1)$. For (I), use continuity of $\partial_\theta \psi(\cdot; \theta, \eta_0)$ in θ in L_1/L_2 (Assumption 2.3,

last sentence) and the fact that $\tilde{\theta}_k$ lies between θ_0 and $\hat{\theta}_k$; since we will show below that $\hat{\theta}_k - \theta_0 = o_p(1)$, it follows that $(I) = o_p(1)$. Altogether, $\hat{A}_k(\tilde{\theta}_k) \rightarrow_p A$ and thus $\hat{A}_k(\tilde{\theta}_k)^{-1} \rightarrow_p A^{-1}$.

Step 4 (Consistency and rate). Insert Step 2 into (A.9):

$$\hat{\theta}_k - \theta_0 = -\hat{A}_k(\tilde{\theta}_k)^{-1} \cdot \frac{1}{|B_k|} \sum_{t \in B_k} \psi(W_t; \theta_0, \eta_0) + \hat{A}_k(\tilde{\theta}_k)^{-1} o_p(|B_k|^{-1/2}).$$

Since $\hat{A}_k(\tilde{\theta}_k)^{-1} = O_p(1)$ by Step 3 and, by Assumption 2.2 (CLT at $u = 1$ on block B_k),

$$\frac{1}{|B_k|} \sum_{t \in B_k} \psi(W_t; \theta_0, \eta_0) = O_p(|B_k|^{-1/2}),$$

we obtain

$$\hat{\theta}_k - \theta_0 = O_p(|B_k|^{-1/2}).$$

In particular, $\hat{\theta}_k - \theta_0 = o_p(1)$, validating the use of continuity in (I) in Step 3.

Step 5 (Linearization). Multiply the display in Step 4 by $\sqrt{|B_k|}$ and apply Slutsky's theorem using $\hat{A}_k(\tilde{\theta}_k)^{-1} \rightarrow_p A^{-1}$ from Step 3:

$$\sqrt{|B_k|}(\hat{\theta}_k - \theta_0) = A^{-1} \cdot \frac{1}{\sqrt{|B_k|}} \sum_{t \in B_k} \psi(W_t; \theta_0, \eta_0) + o_p(1).$$

Uniformity over k holds because K is fixed and all $o_p(\cdot)$ terms above are uniform in k . \square

Proof of Theorem 2.1

PROOF. Step 1 (Linearization). From Lemma 2.2, for each fold k ,

$$\sqrt{|B_k|}(\hat{\theta}_k - \theta_0) = A^{-1} \cdot \frac{1}{\sqrt{|B_k|}} \sum_{t \in B_k} \psi(W_t; \theta_0, \eta_0) + o_p(1),$$

where the $o_p(1)$ term is uniform in k . Equivalently,

$$\hat{\theta}_k - \theta_0 = A^{-1} \cdot \frac{1}{|B_k|} \sum_{t \in B_k} \psi(W_t; \theta_0, \eta_0) + o_p(|B_k|^{-1/2}).$$

Step 2 (Average over folds). Taking the average over $k = 1, \dots, K$,

$$\hat{\theta} - \theta_0 = A^{-1} \cdot \frac{1}{K} \sum_{k=1}^K \frac{1}{|B_k|} \sum_{t \in B_k} \psi(W_t; \theta_0, \eta_0) + \frac{1}{K} \sum_{k=1}^K o_p(|B_k|^{-1/2}).$$

Since K is fixed and the remainders are uniform in k (Lemma 2.2), and $|B_k| \asymp T$ for each k , we have

$$\frac{1}{K} \sum_{k=1}^K o_p(|B_k|^{-1/2}) = o_p(T^{-1/2}).$$

Define $\bar{m}_k := |B_k|^{-1} \sum_{t \in B_k} \psi(W_t; \theta_0, \eta_0)$. Then

$$\hat{\theta} - \theta_0 = A^{-1} \cdot \frac{1}{K} \sum_{k=1}^K \bar{m}_k + o_p(T^{-1/2}).$$

Step 3 (Block average equals full-sample average). Write

$$\frac{1}{K} \sum_{k=1}^K \bar{m}_k = \sum_{k=1}^K \frac{|B_k|}{T} \bar{m}_k + \sum_{k=1}^K \left(\frac{1}{K} - \frac{|B_k|}{T} \right) \bar{m}_k =: (I) + (II).$$

For term (I): Since the blocks partition $\{1, \dots, T\}$ up to $O(1)$ edge effects (Assumption 2.5),

$$(I) = \frac{1}{T} \sum_{t=1}^T \psi(W_t; \theta_0, \eta_0) + O(T^{-1}).$$

For term (II): By construction (Assumption 2.5), $|B_k| = \lfloor T/K \rfloor + O(1) = T/K + O(1)$, so

$$\left| \frac{1}{K} - \frac{|B_k|}{T} \right| = \frac{||B_k| - T/K|}{T} = \frac{O(1)}{T} = O(T^{-1}).$$

By the invariance principle (Assumption 2.2) applied to each block and the mean-zero property $\mathbb{E}[\psi(W_t; \theta_0, \eta_0)] = 0$,

$$\bar{m}_k = O_p(|B_k|^{-1/2}) = O_p(T^{-1/2}).$$

Therefore, with K fixed,

$$|(II)| \leq \sum_{k=1}^K O(T^{-1}) \cdot O_p(T^{-1/2}) = K \cdot O_p(T^{-3/2}) = o_p(T^{-1/2}).$$

Combining,

$$\frac{1}{K} \sum_{k=1}^K \bar{m}_k = \frac{1}{T} \sum_{t=1}^T \psi(W_t; \theta_0, \eta_0) + o_p(T^{-1/2}).$$

Step 4 (Asymptotic normality). We have shown

$$\sqrt{T}(\hat{\theta} - \theta_0) = A^{-1} \cdot \frac{1}{\sqrt{T}} \sum_{t=1}^T \psi(W_t; \theta_0, \eta_0) + o_p(1).$$

By Assumption 2.2, the functional central limit theorem at $u = 1$ gives

$$\frac{1}{\sqrt{T}} \sum_{t=1}^T \psi(W_t; \theta_0, \eta_0) \Rightarrow \mathcal{N}(0, \Sigma).$$

Since A is nonsingular, by Slutsky's theorem and the continuous mapping theorem,

$$\sqrt{T}(\hat{\theta} - \theta_0) \Rightarrow \mathcal{N}(0, A^{-1} \Sigma A^{-1}).$$

□

Supplementary Appendix for “Double Machine Learning for Time Series”

MILOS CIGANOVIC[†], FEDERICO D’AMARIO[†] AND MASSIMILIANO TANCIONI[†]

[†]*Sapienza University of Rome*

*E-mail: milos.ciganovic@uniroma1.it; federico.damario@uniroma1.it;
massimiliano.tancioni@uniroma1.it*

Summary This Supplementary Material for “Double Machine Learning for Time Series” provides formal verification of the assumptions supporting the asymptotic theory and details the data-generating processes used in the paper. It reports extensive Monte Carlo evidence for the Reverse Cross-Fitting estimator under approximately sparse partially linear regression designs, considering both correctly specified and misspecified structural VARs. The simulations compare alternative hyperparameter tuning criteria and show that the Goldilocks-zone metric delivers improved bias properties relative to RMSE-based calibration. We also evaluate the finite-sample performance of Reverse Cross-Fitting relative to Neighbours-Left-Out cross-fitting and assess its robustness to violations of time reversibility induced by GARCH-type heteroskedasticity. The appendix includes results from adapting the methodology to Local Projections, an empirical comparison of estimated regulatory-capital shocks with narrative shocks from the literature, RMSE-calibrated empirical results, and a description of the data sources.

Additional materials include results for Local Projections, an empirical comparison of our estimated regulatory-capital shocks with narrative shocks from the literature, RMSE-calibrated empirical estimates, and a description of the data sources.

Keywords: *Causal Inference, Double Machine Learning, Time Series, Cross-Fitting, Hyperparameters tuning, Local Projections.*

S1. VARIANCE ESTIMATION

From Theorem 2.1

$$\sqrt{T}(\hat{\theta} - \theta_0) \Rightarrow \mathcal{N}(0, V), \quad V := A^{-1}\Sigma A^{-1},$$

so that $\text{Var}(\hat{\theta}) \approx V/T$. Here $A = \mathbb{E}[\partial_{\theta}\psi(W_t; \theta_0, \eta_0)]$ and Σ is the long-run variance of the oracle score process.

For each observation $t = 1, \dots, T$, let (χ_t^k, ξ_t^k) denote the cross-fitted residualized outcome and policy variable, obtained using the nuisance estimates $\hat{\eta}^{(k(t))}$ from the fold $k(t)$ that does not include t in its main block. These residuals are stacked in their original time order across all folds, yielding a single series $(\chi_t, \xi_t)_{t=1}^T$ covering the entire sample. At the final estimate $\hat{\theta}$, define

$$\hat{\epsilon}_t = \chi_t - \hat{\theta} \xi_t, \quad \hat{s}_t = \xi_t \hat{\epsilon}_t,$$

which is the stacked, time-ordered score process (scalar when $d = 1$) that preserves the serial dependence of the underlying data.

Estimate the Jacobian by

$$\hat{A} := \frac{1}{T} \sum_{t=1}^T \partial_{\theta}\psi(W_t; \hat{\theta}, \hat{\eta}^{(k(t))}),$$

which in residual-on-residual OLS reduces to $\hat{A} = T^{-1} \sum_{t=1}^T \xi_t^2$.

Because the stacked score series may be serially correlated (even across folds), an HAC estimator is required. Let $\bar{s} = T^{-1} \sum_{t=1}^T \hat{s}_t$ and, for $h \geq 0$,

$$\hat{\Gamma}(h) = \frac{1}{T} \sum_{t=h+1}^T (\hat{s}_t - \bar{s})(\hat{s}_{t-h} - \bar{s})^\top.$$

Given a kernel $k(\cdot)$ and bandwidth H_T , form the HAC estimator

$$\hat{\Sigma} = \hat{\Gamma}(0) + 2 \sum_{h=1}^{H_T} k\left(\frac{h}{H_T}\right) \hat{\Gamma}(h).$$

This construction aggregates within- and cross-fold serial correlations of the stacked score sequence. The asymptotic covariance is then estimated by

$$\widehat{\text{Var}}(\sqrt{T}(\hat{\theta} - \theta_0)) = \hat{A}^{-1} \hat{\Sigma} \hat{A}^{-1},$$

so that

$$\widehat{\text{Var}}(\hat{\theta}) = \frac{1}{T} \hat{A}^{-1} \hat{\Sigma} \hat{A}^{-1}, \quad \text{SE}(\hat{\theta}) = \sqrt{\frac{1}{T} \hat{A}^{-1} \hat{\Sigma} \hat{A}^{-1}}.$$

We can concisely demonstrate why this is the case. Let $s_t^* := \psi(W_t; \theta_0, \eta_0)$ denote the oracle score for a scalar policy variable. Under Assumptions 2.3–2.4 and fixed K ,

$$\frac{1}{T} \sum_{t=1}^T \mathbb{E} \|\hat{s}_t - s_t^*\|^2 = o_p(T^{-1/2}),$$

and uniformly for $0 \leq h \leq H_T$ with $H_T/T \rightarrow 0$,

$$\max_{0 \leq h \leq H_T} \left\| \frac{1}{T} \sum_{t=h+1}^T \left[(\hat{s}_t - \bar{s})(\hat{s}_{t-h} - \bar{s})^\top - (s_t^* - \bar{s}^*)(s_{t-h}^* - \bar{s}^*)^\top \right] \right\| = o_p(1),$$

where $\bar{s}^* = T^{-1} \sum_t s_t^*$. Hence, the HAC estimator computed from $\{\hat{s}_t\}$ is asymptotically equivalent to that based on $\{s_t^*\}$ following standard HAC arguments (Andrews, 1991; Newey and West, 1987)

Finally, by the kernel-HAC consistency results applied to the oracle score under Assumptions 2.1–2.2, and a bandwidth satisfying $H_T \rightarrow \infty$ and $H_T/T \rightarrow 0$ (e.g., $H_T = o(T^{1/4})$),

$$\hat{\Sigma} \xrightarrow{p} \Sigma, \quad \hat{A} \xrightarrow{p} A, \quad \Rightarrow \quad \hat{A}^{-1} \hat{\Sigma} \hat{A}^{-1} \xrightarrow{p} A^{-1} \Sigma A^{-1}.$$

$\widehat{\text{Var}}(\hat{\theta}) = T^{-1} \hat{A}^{-1} \hat{\Sigma} \hat{A}^{-1}$ is consistent, and the reported standard errors are asymptotically valid.

S2. VERIFICATION OF ASSUMPTIONS

Verification of Assumption 2.2 Assumption 2.2 requires that the partial-sum process of the oracle score $\psi_t^* = \psi(W_t; \theta_0, \eta_0)$ satisfies a functional central limit theorem (FCLT) in $D([0, 1]; \mathbb{R}^d)$:

$$T^{-1/2} \sum_{t=1}^{\lfloor uT \rfloor} \psi_t^* \Rightarrow \mathcal{W}(u), \quad \mathbb{E}[\mathcal{W}(u)\mathcal{W}(v)^\top] = (u \wedge v) \Sigma.$$

This invariance principle ensures that $\sqrt{T}(\hat{\theta} - \theta_0)$ is asymptotically normal in Theorem 2.1. We now provide sufficient conditions for the FCLT and verify that the DGPs considered in Sections 3–4 satisfy them. Rather than imposing strong-mixing restrictions, our assumption can be verified employing the *Maxwell–Woodroffe* (Maxwell and Woodroffe 2000) projective criterion, a weaker and more easily verifiable sufficient condition for the FCLT. Let $S_T = \sum_{t=1}^T \psi_t^*$ and $\mathcal{F}_0 = \sigma(\psi_s^* : s \leq 0)$. If

$$\sum_{T=1}^{\infty} T^{-3/2} \|\mathbb{E}(S_T | \mathcal{F}_0)\|_2 < \infty, \quad (\text{S.1})$$

then $T^{-1/2} \sum_{t \leq uT} \psi_t^* \Rightarrow \mathcal{W}(u)$ in $D([0, 1]; \mathbb{R}^d)$ for a Brownian motion \mathcal{W} with covariance Σ . Condition (S.1) is automatically satisfied for all α -mixing processes with summable mixing coefficients and hence covers a broad class of stationary short-memory sequences. As an example, consider the partially linear regression model

$$y_t = \theta_0 d_t + g_0(X_t) + \epsilon_t, \quad d_t = m_0(X_t) + \xi_t,$$

where $\{X_t\}$ is stationary (for example, a stable Gaussian VAR), and (ϵ_t, ξ_t) are i.i.d. with zero mean and finite fourth moments, independent of $\{X_t\}$. The oracle score entering Assumption 2.2 is

$$\psi_t^* = \{d_t - m_0(X_t)\} \{y_t - \theta_0 d_t - g_0(X_t)\} = \xi_t \epsilon_t.$$

Hence $\{\psi_t^*\}$ is i.i.d. with $\mathbb{E}[\psi_t^*] = 0$ and $\mathbb{E}\|\psi_t^*\|^2 < \infty$, so $\mathbb{E}(S_T | \mathcal{F}_0) = 0$ for all T , and (S.1) holds trivially. Therefore, Assumption 2.2 is verified for the PLR DGP.

Stationary Gaussian linear processes are by definition time-reversible, since their covariance functions satisfy $\Gamma(h) = \Gamma(-h)$ so they satisfy the Maxwell-Woodroffe criterion. This includes both the PLR functions of VAR/SVAR DGPs considered in this paper.

Verification of Assumption 2.4 This section verifies Assumption 2.4 for the partially linear regression (PLR) model used in the paper when the regressor process X_t is a stationary VAR or when (y_t, d_t, X_t) are measurable functions of such a process. We show that the conditional block-average plug-in bias is $o_p(T^{-1/2})$ even though the auxiliary blocks used to train the nuisance estimator $\hat{\eta}^{(k)}$ are adjacent to the main block B_k . Thus, Reverse Cross-Fitting (RCF) does not require temporal gaps.

Let X_t follow a stable Gaussian VAR(p),

$$X_t = \Phi_1 X_{t-1} + \cdots + \Phi_p X_{t-p} + u_t, \quad u_t \stackrel{i.i.d.}{\sim} \mathcal{N}(0, \Sigma_u),$$

with spectral radius strictly smaller than one. The process $\{X_t\}$ is covariance stationary, ergodic, and time-reversible. The PLR model is

$$y_t = \theta_0 d_t + g_0(X_t) + \epsilon_t, \quad d_t = m_0(X_t) + \xi_t,$$

where (ϵ_t, ξ_t) are i.i.d. with zero mean and finite $4 + \delta$ moments and are independent of $\{X_s\}_{s \in \mathbb{Z}}$. For the orthogonal PLR score

$$\psi(W_t; \theta, \eta) = \{d_t - m(X_t)\} \{y_t - \theta d_t - g(X_t)\}, \quad \eta = (g, m),$$

the oracle score is

$$\psi_t^* := \psi(W_t; \theta_0, \eta_0) = \xi_t \epsilon_t.$$

Fix a fold k and write

$$\Delta m_t := \hat{m}^{(k)}(X_t) - m_0(X_t), \quad \Delta g_t := \hat{g}^{(k)}(X_t) - g_0(X_t).$$

Using $d_t = m_0(X_t) + \xi_t$ and $y_t = \theta_0 d_t + g_0(X_t) + \epsilon_t$, we obtain

$$d_t - \hat{m}^{(k)}(X_t) = (m_0(X_t) + \xi_t) - \hat{m}^{(k)}(X_t) = \xi_t - \Delta m_t,$$

and

$$y_t - \theta_0 d_t - \hat{g}^{(k)}(X_t) = (\theta_0 d_t + g_0(X_t) + \epsilon_t) - \theta_0 d_t - \hat{g}^{(k)}(X_t) = \epsilon_t - \Delta g_t.$$

Therefore, the plug-in score can be written as

$$\psi(W_t; \theta_0, \hat{\eta}^{(k)}) = (d_t - \hat{m}^{(k)}(X_t))(y_t - \theta_0 d_t - \hat{g}^{(k)}(X_t)) = (\xi_t - \Delta m_t)(\epsilon_t - \Delta g_t).$$

Expanding the product yields

$$(\xi_t - \Delta m_t)(\epsilon_t - \Delta g_t) = \xi_t \epsilon_t - \xi_t \Delta g_t - \epsilon_t \Delta m_t + \Delta m_t \Delta g_t.$$

Since the oracle score is $\psi_t^* = \xi_t \epsilon_t$, subtracting it gives

$$\psi(W_t; \theta_0, \hat{\eta}^{(k)}) - \psi_t^* = -\xi_t \Delta g_t - \epsilon_t \Delta m_t + \Delta m_t \Delta g_t. \quad (\text{S.2})$$

The first two terms have mean zero because (ϵ_t, ξ_t) are independent of $(X_t, \mathcal{F}_{\text{aux},k})$. Conditioning on $\mathcal{F}_{\text{aux},k}$ and using independence of (ϵ_t, ξ_t) ,

$$\mathbb{E}[\xi_t \Delta g_t \mid \mathcal{F}_{\text{aux},k}, X_t] = \Delta g_t \mathbb{E}[\xi_t] = 0, \quad \mathbb{E}[\epsilon_t \Delta m_t \mid \mathcal{F}_{\text{aux},k}, X_t] = \Delta m_t \mathbb{E}[\epsilon_t] = 0.$$

Taking the conditional expectation of (S.2) therefore, gives

$$\mathbb{E}[\psi(W_t; \theta_0, \hat{\eta}^{(k)}) - \psi_t^* \mid \mathcal{F}_{\text{aux},k}] = \mathbb{E}[\Delta m_t \Delta g_t \mid \mathcal{F}_{\text{aux},k}]. \quad (\text{S.3})$$

By Cauchy-Schwarz and stationarity of X_t ,

$$|\mathbb{E}[\Delta m_t \Delta g_t \mid \mathcal{F}_{\text{aux},k}]| \leq (\mathbb{E}[\Delta m_t^2 \mid \mathcal{F}_{\text{aux},k}])^{1/2} (\mathbb{E}[\Delta g_t^2 \mid \mathcal{F}_{\text{aux},k}])^{1/2} = \|\hat{m}^{(k)} - m_0\|_{L_2} \|\hat{g}^{(k)} - g_0\|_{L_2}. \quad (\text{S.4})$$

Since stationarity implies the same bound holds for all $t \in B_k$, averaging (S.3) over $t \in B_k$ yields

$$\left\| \mathbb{E} \left[\frac{1}{|B_k|} \sum_{t \in B_k} \{\psi(W_t; \theta_0, \hat{\eta}^{(k)}) - \psi_t^*\} \mid \mathcal{F}_{\text{aux},k} \right] \right\| \leq \|\hat{m}^{(k)} - m_0\|_{L_2} \|\hat{g}^{(k)} - g_0\|_{L_2}. \quad (\text{S.5})$$

Assumption 2.4 of the paper requires that, uniformly in k ,

$$\|\hat{m}^{(k)} - m_0\|_{L_2} = o_p(T^{-1/4}), \quad \|\hat{g}^{(k)} - g_0\|_{L_2} = o_p(T^{-1/4}).$$

Then the right-hand side of (S.5) satisfies

$$\|\hat{m}^{(k)} - m_0\|_{L_2} \|\hat{g}^{(k)} - g_0\|_{L_2} = o_p(T^{-1/2}),$$

so the conditional plug-in bias obeys

$$\left\| \mathbb{E} \left[\frac{1}{|B_k|} \sum_{t \in B_k} \{\psi(W_t; \theta_0, \hat{\eta}^{(k)}) - \psi_t^*\} \mid \mathcal{F}_{\text{aux},k} \right] \right\| = o_p(T^{-1/2}),$$

which verifies the conditional stability requirement of Assumption 2.4. Notably, this argument does not require any temporal separation between B_k and the auxiliary blocks.

We can extend this to the SVAR(p) case, since invertibility of the VAR implies that (ϵ_t, ξ_t) are linear combinations of the i.i.d. shocks ϵ_t and thus independent of the lagged state. The algebra of (S.2), (S.3), and (S.4) holds verbatim, implying that (S.5) and the $o_p(T^{-1/2})$ conclusion continue to hold. Hence, Assumption 2.4 is satisfied whenever the

nuisance estimators achieve the $o_p(T^{-1/4})$ L_2 rates. For PLR models driven by stationary VAR or SVAR processes, the conditional stability requirement follows directly from the orthogonal score structure and the L_2 rates of the nuisance estimators. Therefore, Reverse Cross-Fitting does not require temporal gaps between main and auxiliary blocks, and inference remains valid under serial dependence.

S3. SIMULATION SETUP

We present simulation evidence on the performance of RCF-DML under two DGPs: a contemporaneously recursive SVAR and a PLR model.¹ In addition, we assess the bias-reduction properties of the proposed “Goldilocks zone” tuning metric relative to standard predictive metrics, such as RMSE. For both DGPs, we consider $p = 100$ covariance stationary variables, and the estimated PLR model is:

$$y_t = \theta d_t + g_0(X_{i,t}) + \epsilon_t, \quad E[\epsilon_t | X_t, d_t] = 0, \quad (\text{S.6})$$

$$d_t = m_0(X_{i,t}) + \xi_t, \quad E[\xi_t | X_t] = 0. \quad (\text{S.7})$$

In the case of the SVAR, the setting is defined as follows:

$$Y_t = \mu + \Phi_1 Y_{t-1} + \varepsilon_t, \quad \varepsilon_t = P u_t, \quad u_t \sim \mathcal{N}(0, I_n), \quad (\text{S.8})$$

where $Y_t \in \mathbb{R}^n$ and P is a lower-triangular Cholesky factor encoding contemporaneous impacts. The autoregressive matrix Φ_1 induces approximate sparse local dependence via asymmetric, band-limited decay. For each pair (i, j) with $|i - j| \leq b$,

$$(\Phi_1)_{ij} = \begin{cases} \frac{\kappa}{1 + |i - j|^\alpha} \eta_{ij}, & i > j \quad (\text{below diagonal, slower decay}), \\ \frac{0.6\kappa}{1 + |i - j|^\beta} \eta_{ij}, & i < j \quad (\text{above diagonal, faster decay}), \\ \kappa \eta_{ii}, & i = j, \end{cases}$$

with $\eta_{ij} \sim \text{Unif}(0.8, 1.2)$ introducing mild heterogeneity. The matrix is then rescaled to ensure a spectral radius no greater than $\rho^* = 0.95$:

$$\Phi_1 \leftarrow \Phi_1 \cdot \min \left\{ 1, \frac{\rho^*}{\rho(\Phi_1)} \right\}.$$

The reduced-form covariance matrix is $\Sigma_\varepsilon = P P'$, where P is a lower-triangular matrix with positive diagonal elements generated as

$$P_{ii} \sim \text{Unif}(d_{\min}, d_{\max}), \quad P_{ij} = \frac{\omega \xi_{ij}}{1 + (i - j)^\delta}, \quad j < i,$$

with $\xi_{ij} \sim \text{Unif}(0.4, 1.6)$ and $\omega = 0.7$.

We impose a contemporaneous effect of structural shock i on variable j through

$$P_{ji} = \gamma = 0.5, \quad (i \leq j).$$

¹These DGPs imply that confounders affect the policy and outcome variables through linear functions. CF can also be used with nonlinear nuisance functions, since any time-reversible series remains time-reversible under nonlinear transformations. The main difference between the two DGPs is that the SVAR, unlike the PLR, allows for endogeneity due to reverse causality.

We draw innovations $u_t \sim \mathcal{N}(0, I_n)$, compute $\varepsilon_t = Pu_t$, and generate data for $t = 1, \dots, T+B$ with a burn-in $B = 300$. Only the last T observations are retained. Variables i and j are then used as the policy and outcome variables in the estimated PLR. By varying this pair, we consider two scenarios:

- 1 *Correctly specified PLR model.* Variable i is placed last but one, and variable j last, so the outcome does not enter contemporaneously in the policy equation; all remaining variables serve as contemporaneous controls.
- 2 *Mis-specified PLR model.* Variable i is placed in the middle of the SVAR ordering (with j still last), so only half the control variables are contemporaneously relevant for the policy equation, but the PLR includes all of them at time t .

For the PLR setting, confounders $X_{i,t}$ follow a VAR(1) process with a diagonal autoregressive matrix with $\rho_i \in \{0.05, 0.9\}$ to capture low- and high-memory regimes. We additionally consider two correlation structures: no correlation ($cor = 0$) and positive correlation ($cor = 0.7$). The covariance matrix is:

$$\Omega = cor^{|i-j|} \quad \text{with } i, j = 1, \dots, 50.$$

The policy and outcome equations are:

$$d_t = X_{i,t}\beta + \xi_t, \quad \xi_t \sim \mathcal{N}(0, 1) \tag{S.9}$$

$$y_t = 0.5d_t + X_{i,t}\gamma + \varepsilon_t, \quad \varepsilon_t \sim \mathcal{N}(0, 1) \tag{S.10}$$

with approximate sparse coefficients

$$\beta_i = \nu_i(1/i)^2, \quad \gamma_i = \zeta_i(2/i)^2, \quad \text{with } \nu_i, \zeta_i \sim \text{Beta}(1, 0.7), \quad \zeta_i \sim \text{Beta}(0.25, 0.8).$$

These DGPs accommodate a wide range of empirical macroeconomic environments in which no distinct pattern of sparsity is evident, such that no predictor can be reliably excluded (Giannone et al., 2021).

We estimate the nuisance functions using Lasso for the SVAR DGP and Elastic Net for the PLR DGP. For the SVAR setting, the tuning grid consists of ten linearly spaced regularization parameters $\alpha \in [0.1, 1]$. For the PLR setting, we use a finer grid, $\alpha \in [0.01, 0.1]$, and fix the Elastic Net mixing parameter at an L_1 -ratio of 0.99.² We conduct 10000 Monte Carlo simulations for each combination of DGP setting.

The total computation time for all simulations and the empirical application was seven hours, 25 minutes, 20 seconds on a machine equipped with two Intel Xeon Platinum 8480+ 2.0 GHz processors (112 physical cores) and 256 GB of RAM.

²We use Lasso for the SVAR DGP and Elastic Net for the PLR DGP because the two designs exhibit fundamentally different sparsity structures. The SVAR imposes exact zeros through the Cholesky parametrization of P and band-limited decay in Φ_1 , so the nuisance functions are genuinely sparse and well-suited to L_1 shrinkage. By contrast, the PLR DGP produces dense but weak coefficient patterns in (β, γ) , making Lasso too aggressive. For this reason, we estimate the PLR nuisance functions using Elastic Net with an L_1 -ratio of 0.99, which behaves as a near-Lasso but includes a minimal L_2 penalty to stabilise dense signals. We also tune the PLR penalty over a finer and lower grid $\alpha \in [0.01, 0.1]$, which reduces shrinkage intensity relative to the SVAR case and mitigates the overshrinkage that arises when no exact sparsity is present.

S4. SIMULATION RESULTS

S4.1. Partially linear DGP

This section reports the results obtained under the approximately sparse PLR DGP. We first describe the asymptotic properties of this design to clarify the theoretical benchmarks for evaluation, and then examine how different tuning metrics and CF strategies perform in finite samples, emphasizing their relative behaviour across specifications.

S4.1.1. Asymptotic performances Figure S.1 illustrates the asymptotic performance of the RCF estimator for the PLR DGP using a sample size $T = 1000$. The plots show how the 95% coverage probability, percentage bias, and mean standard error vary with different choices of the parameter K .

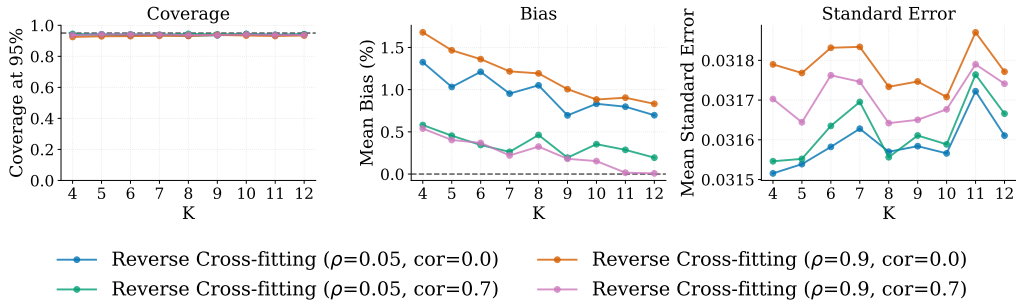


Figure S.1. Asymptotic performance of the Reverse Cross-Fitting estimator for different values of K . The figure reports the estimator’s asymptotic properties for $K \in \{4, \dots, 12\}$, including: (left) the 95% nominal coverage probability, (centre) the mean percentage bias, and (right) the mean HAC standard errors. Results are obtained over 10,000 Monte Carlo replications.

S4.1.2. Metric Comparison Figures S.2 and S.3 show the percentage bias and 95% coverage probabilities obtained using the Goldilocks zone and RMSE tuning metrics. We consider sample sizes $T \in \{50, 100, 200\}$ and multiple values of K .

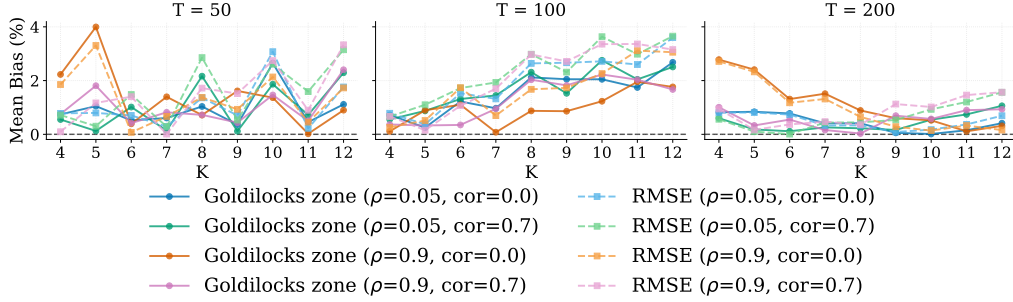


Figure S.2. Comparison of mean bias (%) between Goldilocks zone metric and RMSE using Reverse Cross-fitting. The subplots illustrate the accuracy of the estimator for $K \in \{4, \dots, 12\}$, where Goldilocks zone results are shown with solid lines and dotted markers (blue, green, orange, and purple corresponding to the four (ρ, cor) configurations). In contrast, RMSE results are shown with dashed lines and square markers (light blue, light green, orange, and pink for the same configurations). Panels report performance at different sample sizes: (left) $T = 50$, (centre) $T = 100$, and (right) $T = 200$. Results are obtained over 10,000 Monte Carlo replications.

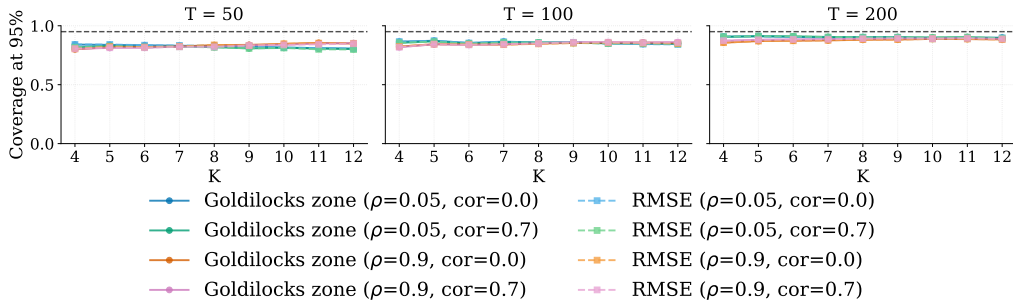


Figure S.3. Comparison of coverage at the 95% level between Goldilocks zone metric and RMSE using Reverse Cross-fitting. The subplots illustrate the coverage of the estimator for $K \in \{4, \dots, 12\}$, where Goldilocks zone results are shown with solid lines and dotted markers (blue, green, orange, and purple corresponding to the four (ρ, cor) configurations), and RMSE results are shown with dashed lines and square markers (light blue, light green, orange, and pink for the same configurations). The panels report results for different sample sizes: (left) $T = 50$, (centre) $T = 100$, and (right) $T = 200$. Results are obtained over 10,000 Monte Carlo replications.

S4.1.3. Method Comparison We compare the performance of the RCF and NLO-DML estimators in small samples with $T \in \{50, 100, 200\}$ under the Approximate Sparse (PLR) DGP. Figures S.4 and S.5 display the percentage bias and 95% coverage probabilities achieved by the two cross-fitting strategies.

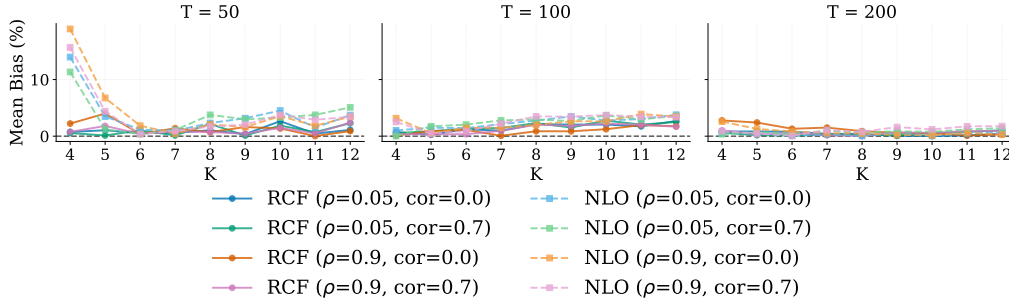


Figure S.4. Comparison of mean bias (%) between RCF and NLO methods. The subplots illustrate the accuracy of the estimator for $K \in \{4, \dots, 12\}$, where RCF results are shown with solid lines and dotted markers (blue, green, orange, and purple corresponding to the four (ρ, cor) configurations), and NLO results are shown with dashed lines and square markers (light blue, light green, orange, and pink for the same configurations). The panels report results for different sample sizes: (left) $T = 50$, (centre) $T = 100$, and (right) $T = 200$. Results are obtained over 10,000 Monte Carlo replications.

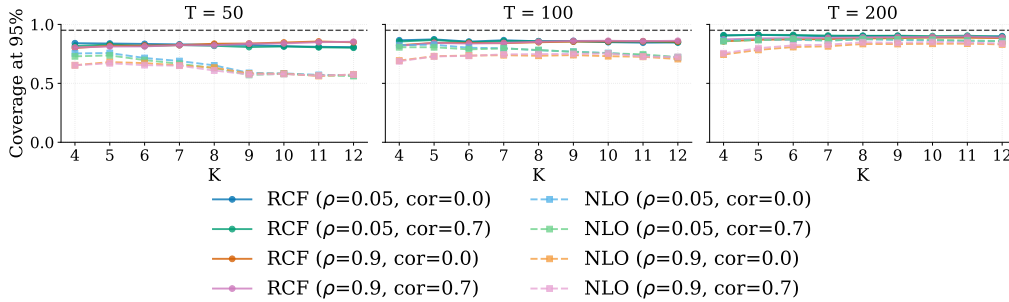


Figure S.5. Comparison of coverage at the 95% level between RCF and NLO methods. The subplots illustrate the coverage of the estimator for $K \in \{4, \dots, 12\}$, where RCF results are shown with solid lines and dotted markers (blue, green, orange, and purple corresponding to the four (ρ, cor) configurations), and NLO results are shown with dashed lines and square markers (light blue, light green, orange, and pink for the same configurations). The panels report results for different sample sizes: (left) $T = 50$, (centre) $T = 100$, and (right) $T = 200$. Results are obtained over 10,000 Monte Carlo replications.

S4.2. Correctly Specified SVAR DGP

We next evaluate the performance of the RCF-DML estimator under the Correctly Specified SVAR DGP. In this configuration, the imposed ordering guarantees that only contemporaneous controls relevant to the true DGP are included: variable i is ordered last but one, and variable j is placed last, ensuring that the outcome variable does not appear contemporaneously in the policy equation. All remaining variables function as contemporaneous controls, aligning the empirical specification with the structural restrictions of the DGP.

S4.2.1. Asymptotic performances Figure S.6 illustrates the asymptotic performance of the Reverse Cross-fitting estimator for the *correctly-specified* SVAR, using a sample size of $T = 1000$. The plots show how the 95% coverage probability, percentage bias, and mean standard error vary with different choices of the parameter K .

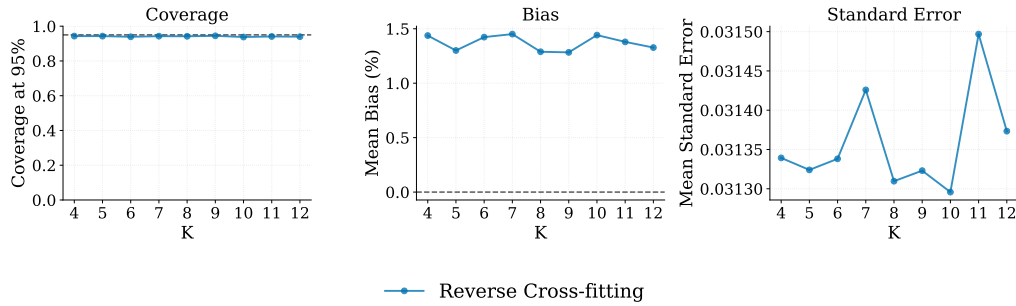


Figure S.6. Asymptotic performance of the Reverse Cross-Fitting estimator for different values of K . The figure reports the estimator's asymptotic properties for $K \in \{4, \dots, 12\}$, including: (left) the 95% nominal coverage probability, (centre) the mean percentage bias, and (right) the mean HAC standard errors. Results are obtained over 10,000 Monte Carlo replications.

S4.2.2. Metric Comparison Figures S.7 and S.8 show the percentage bias and 95% coverage probabilities achieved using the Goldilocks zone and RMSE tuning metrics. We consider sample sizes $T \in \{50, 100, 200\}$ and various choices of K .

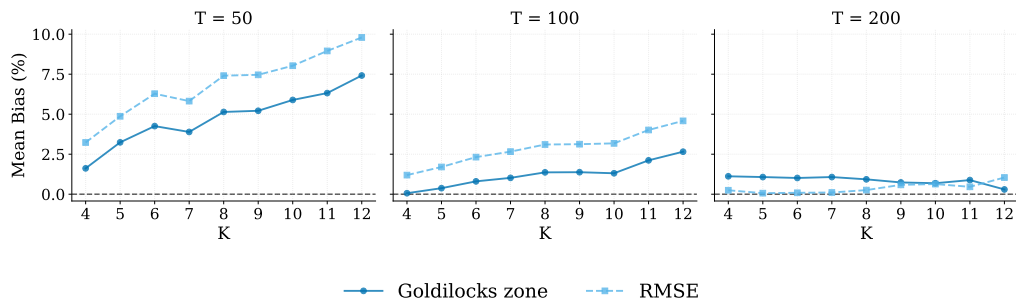


Figure S.7. Comparison of mean bias (%) between Goldilocks zone metric and RMSE using Reverse Cross-fitting. The subplots illustrate the accuracy of the estimator employing Goldilocks zone metric (solid blue line with dots) and RMSE (dashed light blue line with squares) for $K \in \{4, \dots, 12\}$ evaluated at different sample sizes: (left) $T = 50$, (centre) $T = 100$, and (right) $T = 200$. Results are obtained over 10,000 Monte Carlo replications.

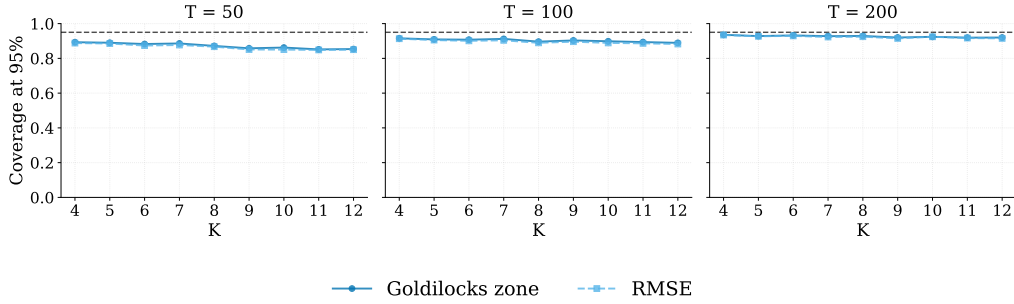


Figure S.8. Comparison of coverage at the 95% level between Goldilocks zone metric and RMSE using Reverse Cross-fitting. The subplots illustrate the coverage of the estimator employing Goldilocks zone metric (solid blue line with dots) and RMSE (dashed light blue line with squares) for $K \in \{4, \dots, 12\}$ evaluated at different sample sizes: (left) $T = 50$, (centre) $T = 100$, and (right) $T = 200$. Results are obtained over 10,000 Monte Carlo replications.

S4.2.3. Method Comparison We compare the relative performance of the RCF and NLO-DML estimators in small samples, $T \in \{50, 100, 200\}$, under the Correctly Specified SVAR DGP. Figures S.9 and S.10 show the percentage bias and 95% coverage probabilities obtained using the two cross-fitting designs.

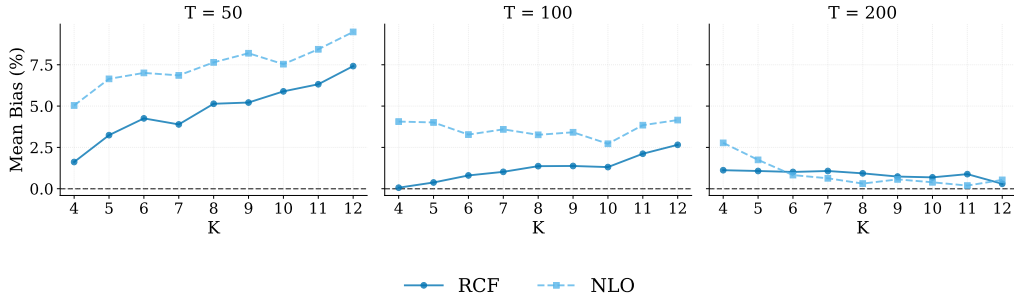


Figure S.9. Comparison of mean bias (%) between RCF and NLO methods. The subplots illustrate the accuracy of RCF (solid blue line with dots) and NLO (dashed light blue line with squares) for $K \in \{4, \dots, 12\}$ evaluated at different sample sizes: (left) $T = 50$, (centre) $T = 100$, and (right) $T = 200$. Results are obtained over 10,000 Monte Carlo replications.

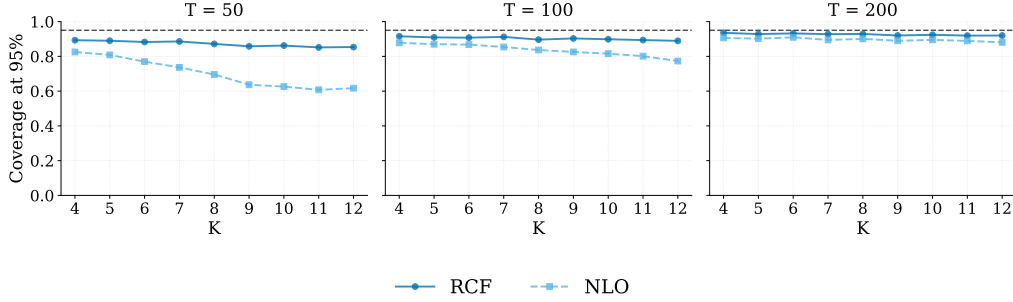


Figure S.10. Comparison of coverage at the 95% level between RCF and NLO methods. The subplots illustrate the coverage of the estimator employing RCF (solid blue line with dots) and NLO (dashed light blue line with squares) for $K \in \{4, \dots, 12\}$ evaluated at different sample sizes: (left) $T = 50$, (centre) $T = 100$, and (right) $T = 200$. Results are obtained over 10,000 Monte Carlo replications.

S4.3. GARCH-SVAR DGP

We consider a case in which a key requirement of RCF-DML is violated: the time-reversibility condition. We break this assumption by introducing GARCH heteroskedasticity. Specifically, we modify the stochastic structure of the structural shocks to feature time-varying conditional variances governed by n independent GARCH(1,1) processes. Each structural shock is now defined as

$$u_{i,t} = \sqrt{h_{i,t}} z_{i,t}, \quad z_{i,t} \sim \mathcal{N}(0, 1),$$

where the conditional variance $h_{i,t}$ evolves according to

$$h_{i,t} = \omega_i + \alpha_i u_{i,t-1}^2 + \beta_i h_{i,t-1}, \quad i = 1, \dots, n.$$

Identical GARCH(1,1) parameters govern each conditional variance process:

$$\omega_i = 0.05, \quad \alpha_i = 0.10, \quad \beta_i = 0.85, \quad i = 1, \dots, n,$$

which satisfy the covariance-stationarity conditions of the DGP and preserve the overall stability of the SVAR.

S4.3.1. Mis-specified GARCH-SVAR DGP Figures S.11 and S.12 report the percentage bias and the 95% coverage of the DML estimator obtained with the RCF and NLO cross-fitting designs when the homoskedasticity, and therefore the time-reversibility assumption, is severely violated.

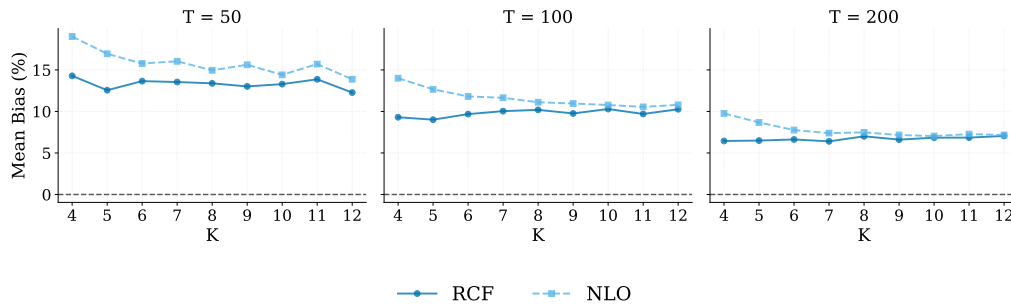


Figure S.11. Comparison of mean bias (%) between RCF and NLO methods under GARCH heteroskedasticity (violation of time reversibility). The subplots illustrate the accuracy of RCF (solid blue line with dots) and NLO (dashed light blue line with squares) for $K \in \{4, \dots, 12\}$ evaluated at different sample sizes: (left) $T = 50$, (centre) $T = 100$, and (right) $T = 200$. Results are obtained over 10,000 Monte Carlo replications.

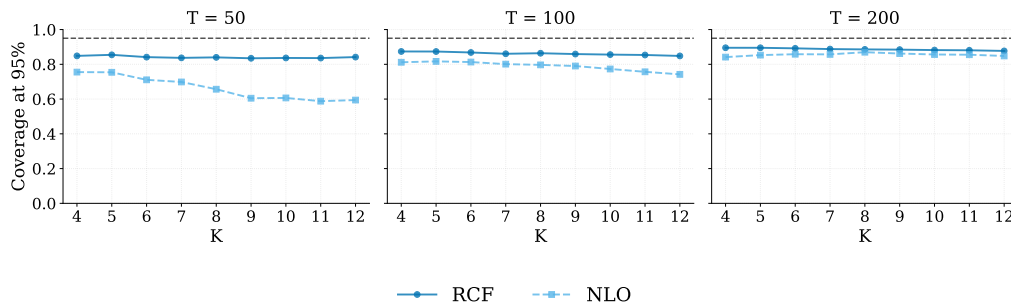


Figure S.12. Comparison of coverage at the 95% level between RCF and NLO methods under GARCH heteroskedasticity (violation of time reversibility). The subplots illustrate the coverage of the estimator employing RCF (solid blue line with dots) and NLO (dashed light blue line with squares) for $K \in \{4, \dots, 12\}$ evaluated at different sample sizes: (left) $T = 50$, (centre) $T = 100$, and (right) $T = 200$. Results are obtained over 10,000 Monte Carlo replications.

S4.3.2. Correctly Specified GARCH-SVAR DGP Figures S.13 and S.14 display the percentage bias and the 95% coverage probabilities of the DML estimator obtained using the RCF and NLO CF designs.

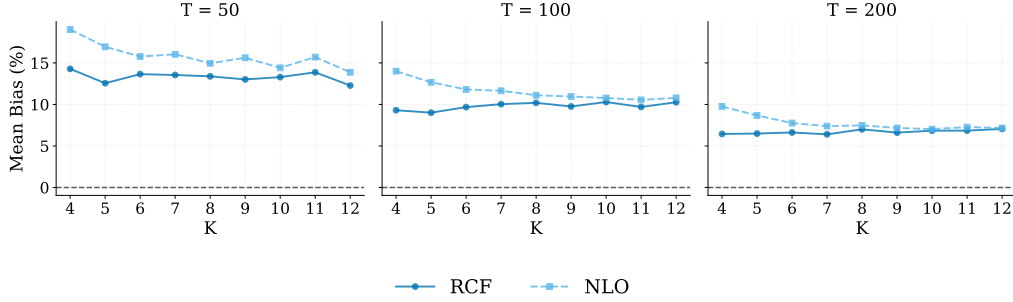


Figure S.13. Comparison of mean bias (%) between RCF and NLO methods under GARCH heteroskedasticity (violation of time reversibility). The subplots illustrate the accuracy of RCF (solid blue line with dots) and NLO (dashed light blue line with squares) for $K \in \{4, \dots, 12\}$ evaluated at different sample sizes: (left) $T = 50$, (centre) $T = 100$, and (right) $T = 200$. Results are obtained over 10,000 Monte Carlo replications.

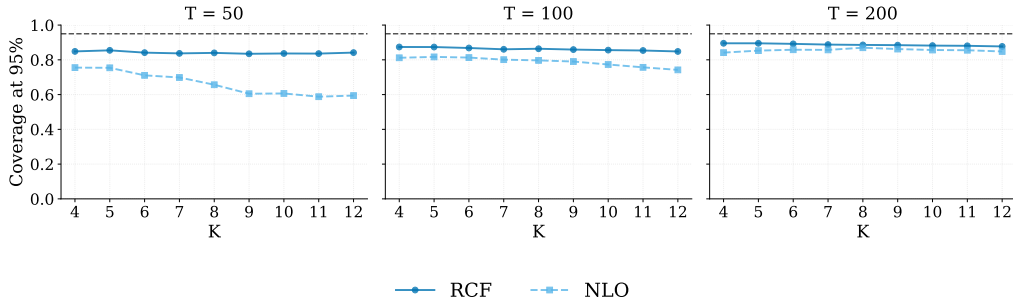


Figure S.14. Comparison of coverage at the 95% level between RCF and NLO methods under GARCH heteroskedasticity (violation of time reversibility). The subplots illustrate the coverage of the estimator employing RCF (solid blue line with dots) and NLO (dashed light blue line with squares) for $K \in \{4, \dots, 12\}$ evaluated at different sample sizes: (left) $T = 50$, (centre) $T = 100$, and (right) $T = 200$. Results are obtained over 10,000 Monte Carlo replications.

S4.4. Local Projections

We show that the RCF-DML methodology can be used to estimate dynamic causal effects. In a dynamic policy evaluation setting, the ground-truth target is the recursive solution of the mis-specified SVAR. The DML-LP model is:

$$y_{t+h} = \theta_h d_t + g_h(X_t) + \epsilon_{t+h}, \quad E[\epsilon_{t+h} | X_t, d_t] = 0, \quad (\text{S.11})$$

$$d_t = m_0(X_t) + \xi_t, \quad E[\xi_t | X_t] = 0, \quad (\text{S.12})$$

for horizons $h = 0, 1, \dots, H$. The dynamic partialling-out equation is:

$$\hat{\chi}_{t+h} = \theta_h \hat{\xi}_t + \epsilon_{t+h}, \quad (h = 0, \dots, 8), \quad (\text{S.13})$$

where

$$\hat{\chi}_{t+h} = y_{t+h} - \hat{g}_h^r(X_t), \quad \hat{\xi}_t = d_t - \hat{m}_0(X_t),$$

and $g_h^r \neq g_h$ denotes the reduced-form mapping for the outcome equation employed in the residualization step.

S4.4.1. Correctly Specified SVAR Figures S.15 and S.16 present the absolute bias and the coverage of the RCF-DML-LP model in estimating the SVAR-based IRFs across eight horizons.

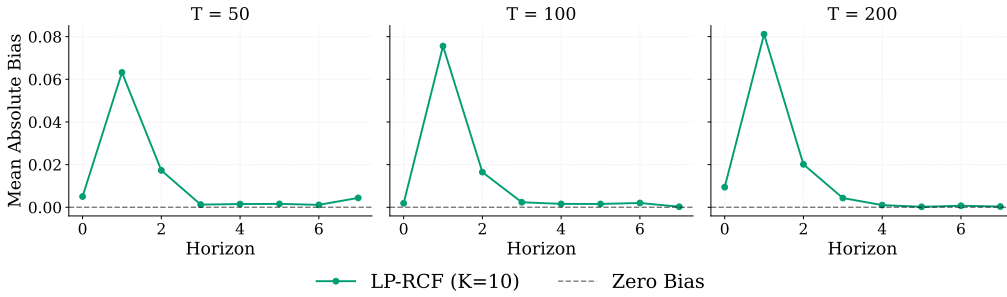


Figure S.15. Mean absolute bias of the LP estimator using the proposed LP-RCF method. The subplots illustrate the mean absolute bias of the estimator across prediction horizons $h \in \{0, \dots, 7\}$ with fixed $K = 10$, evaluated at different sample sizes: (left) $T = 50$, (centre) $T = 100$, and (right) $T = 200$. We report absolute bias rather than percentage bias to avoid numerical divergence (the “exploding percentage” problem) when the true coefficient approaches zero. Results are obtained over 10,000 Monte Carlo replications.

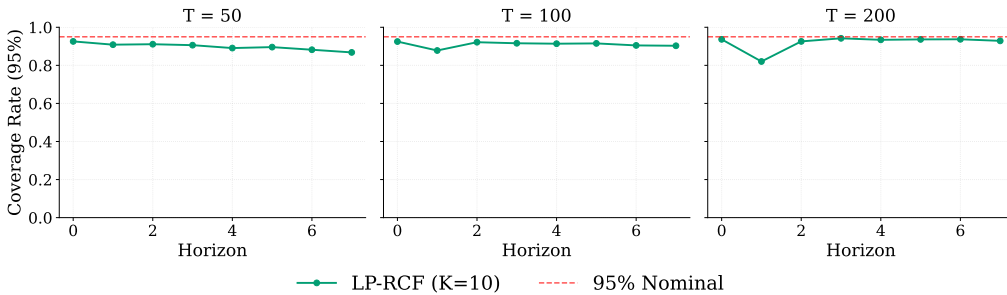


Figure S.16. Comparison of coverage at the 95% level of the LP estimator using the proposed LP-RCF method. The subplots illustrate the coverage of the estimator across prediction horizons $h \in \{0, \dots, 7\}$ with fixed $K = 10$, evaluated at different sample sizes: (left) $T = 50$, (centre) $T = 100$, and (right) $T = 200$. Results are obtained over 10,000 Monte Carlo replications.

S4.4.2. Mis-specified SVAR Figures S.17 and S.18 show the absolute bias and coverage of the RCF-DML-LP estimator in recovering the impulse responses implied by the *mis-specified* SVAR across eight horizons.

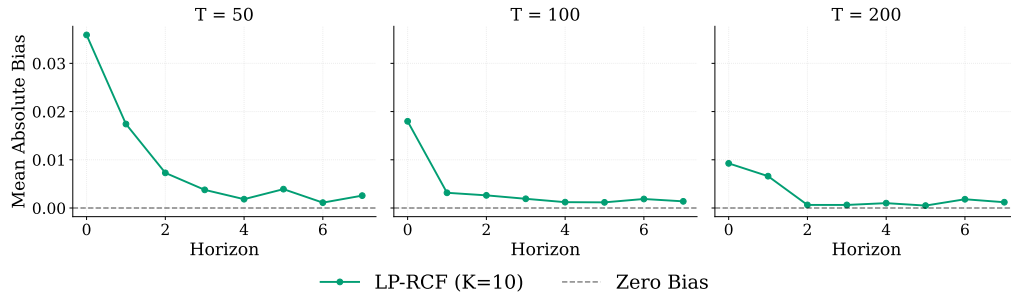


Figure S.17. Mean absolute bias of the LP estimator using the proposed LP-RCF method. The subplots illustrate the mean absolute bias of the estimator across prediction horizons $h \in \{0, \dots, 7\}$ with fixed $K = 10$, evaluated at different sample sizes: (left) $T = 50$, (centre) $T = 100$, and (right) $T = 200$. We report absolute bias rather than percentage bias to avoid numerical divergence (the “exploding percentage” problem) when the true coefficient approaches zero. Results are obtained over 10,000 Monte Carlo replications.

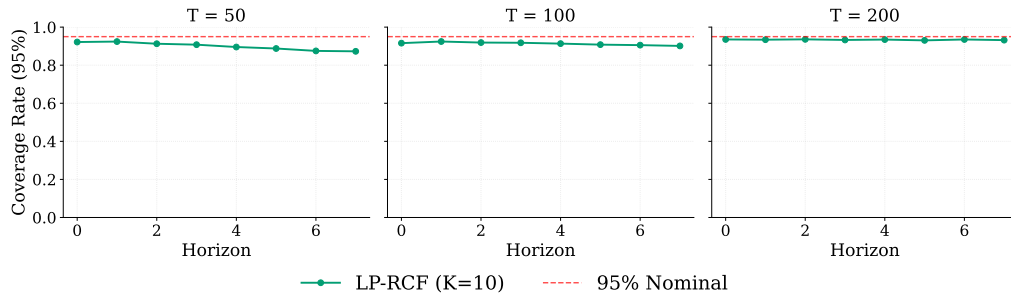


Figure S.18. Comparison of coverage at the 95% level of the LP estimator using the proposed LP-RCF method. The subplots illustrate the coverage of the estimator across prediction horizons $h \in \{0, \dots, 7\}$ with fixed $K = 10$, evaluated at different sample sizes: (left) $T = 50$, (centre) $T = 100$, and (right) $T = 200$. Results are obtained over 10,000 Monte Carlo replications.

S4.5. Neighbours left-out with Goldilocks zone

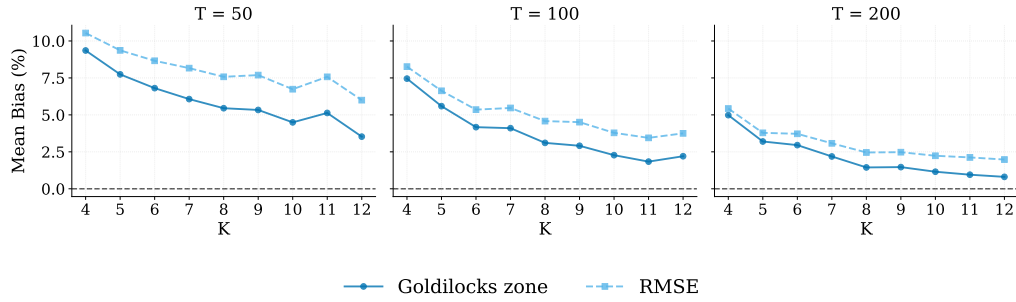


Figure S.19. Comparison of mean bias (%) between Goldilocks zone metric and RMSE using NLO. The subplots illustrate the accuracy of the estimator employing Goldilocks zone metric (solid blue line with dots) and RMSE (dashed light blue line with squares) for $K \in \{4, \dots, 12\}$ evaluated at different sample sizes: (left) $T = 50$, (centre) $T = 100$, and (right) $T = 200$. Results are obtained over 10,000 Monte Carlo replications.

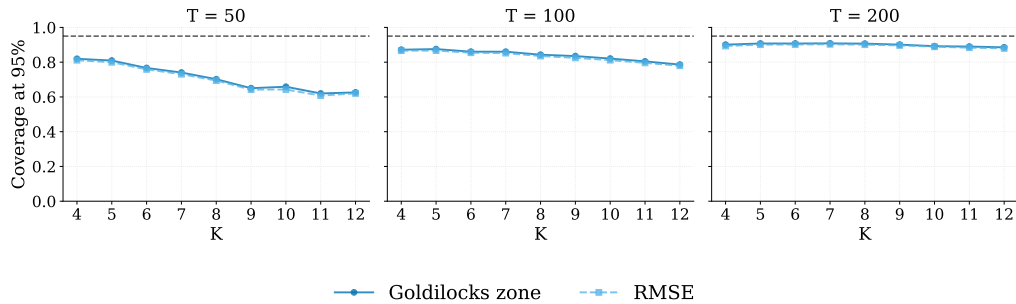


Figure S.20. Comparison of coverage at the 95% level between Goldilocks zone metric and RMSE using NLO. The subplots illustrate the coverage of the estimator employing Goldilocks zone metric (solid blue line with dots) and RMSE (dashed light blue line with squares) for $K \in \{4, \dots, 12\}$ evaluated at different sample sizes: (left) $T = 50$, (centre) $T = 100$, and (right) $T = 200$. Results are obtained over 10,000 Monte Carlo replications.

S5. DATA SOURCES

Table S.1 lists all variables used in the empirical application alongside their sources.

Table S.1. Variables used in Section 5.

Variable Name	Frequency	Source	Type
Tier 1 capital to risk-weighted assets	Q	IMF	Treatment
Real Gross Domestic Product, Reference Year 2020, SA	Q	ISTAT	Outcome
Tier 1 Capital	Q	IMF	Channel
Risk-weighted Assets	Q	IMF	Channel
Secured Loans to domestic households, flow, Reference Year 2020	Q	Bank of Italy	Channel
Loans to domestic PNFC, flow, Reference Year 2020	Q	Bank of Italy	Channel
Household Volume of New Lending	Q	Bank of Italy	Channel
PNFC Volume of New Lending, Reference Year 2020	Q	Bank of Italy	Channel
PNFC interest rate spread	Q	Bank of Italy	Channel
Households interest rate spread	Q	Bank of Italy	Channel
Banks Return-on-Equity	Q	IMF	Control
Provisions to NPLs	Q	IMF	Control
Total Real Exports, Reference Year 2020, SA	Q	ISTAT	Control
Total Real Imports, Reference Year 2020, SA	Q	ISTAT	Control
Households Final Consumption Expenditure, Reference Year 2020, SA	Q	ISTAT	Control
Government Final Consumption Expenditure, Reference Year 2020, SA	Q	ISTAT	Control
Gross Fixed Investments, Reference Year 2020, SA	Q	ISTAT	Control
Unemployment Rate 15-74, SA	Q	ISTAT	Control
Employed 15 and over	Q	ISTAT	Control
FTSE All Shares	Q	Refinitiv	Control
Gross yield of benchmark 3-year BTP	M	Bank of Italy	Control
Gross yield of benchmark 5-year BTP	M	Bank of Italy	Control
Gross yield of benchmark 10-year BTP	M	Bank of Italy	Control
Gross yield of benchmark 30-year BTP	M	Bank of Italy	Control
Gross yield of benchmark CCT	M	Bank of Italy	Control
Gross yield of benchmark 10-year BUND	M	Bank of Italy	Control
Interest rate Spread BTP-BUND 10	M	Bank of Italy	Control
Exchange rates: Pound Sterling/Euro	M	Bank of Italy	Control
Exchange rates: Yen/Euro	M	Bank of Italy	Control
Exchange rates: US Dollar/Euro	M	Bank of Italy	Control
Shadow rate	M	Krippner (2013)	Control

S6. EMPIRICAL APPLICATION

Regulatory capital shock We compare the partialling-out residual of our policy variable with the regulatory capital shocks estimated by Conti et al. (2023) for Italy, who identify the shocks within a structural VAR using sign and magnitude restrictions. Figure S.21 presents the two series over the overlapping sample period covered by both studies.

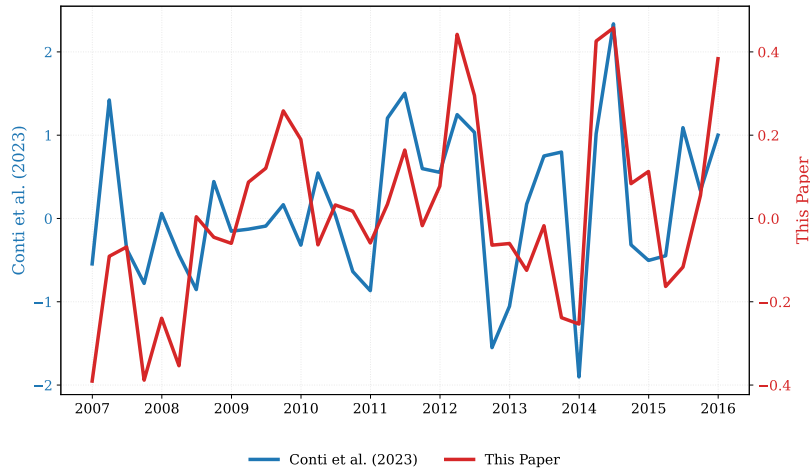


Figure S.21. Comparison of estimated shocks: Conti et al. (2023) vs. this paper.

The comparison shows that the procedure proposed in this paper can isolate the main regulatory shock episodes identified in the existing literature. In particular, our estimated shock series displays a pronounced peak around the onset of discussions that ultimately led to the adoption of the Basel III framework (2009:Q1), as well as around the implementation of the Capital Requirements Directive IV (CRD IV), the European transposition of Basel III. The correlation between our shock series and that of Conti et al. (2023) is approximately 0.55, indicating substantial alignment and confirming the ability of the RCF-DML methodology to recover unexpected movements in the policy variable in a theory-consistent manner.

RMSE Calibration We also report impulse responses estimated via predictive (RMSE-based) calibration of the nuisance functions, highlighting the advantages of the Goldilocks zone metric proposed in the main paper.

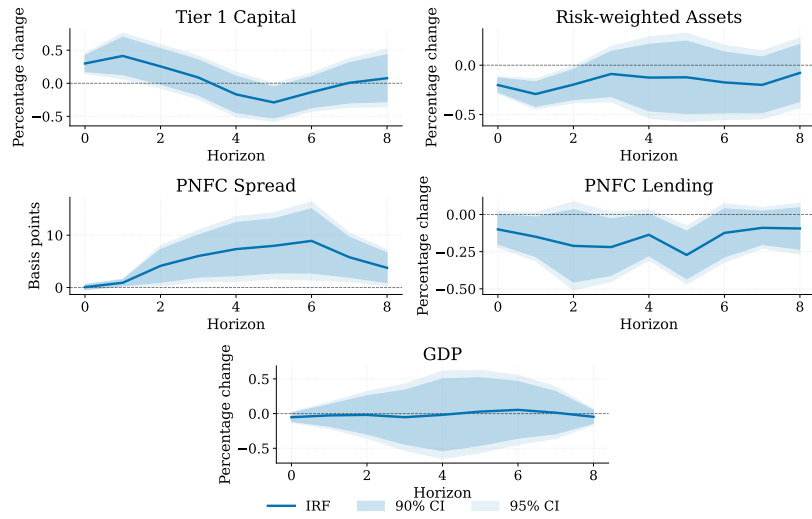


Figure S.22. Cumulative Impulse response function to a regulatory capital shock obtained via RCF-DML employing RMSE metric. The dark (light) blue shaded areas denote 95% (90%) cumulative confidence intervals computed via HAC.

REFERENCES

- Andrews, D. W. K. (1991). Heteroskedasticity and autocorrelation consistent covariance matrix estimation. *Econometrica*, 59(3), 817–858.
- Conti, A. M., Nobili, A., and Signoretti, F. M. (2023). Bank capital requirement shocks: A narrative perspective. *European Economic Review*, 151, 104254.
- Giannone, D., Lenza, M., and Primiceri, G. E. (2021). Economic predictions with big data: The illusion of sparsity. *Econometrica*, 89(5), 2409–2437.
- Krippner, L. (2013). Measuring the stance of monetary policy in zero lower bound environments. *Economics Letters*, 118(1), 135–138.
- Maxwell, M., and Woodroffe, M. (2000). Central limit theorems for additive functionals of Markov chains. *Annals of Probability*, 28(2), 713–724.
- Newey, W. K. and West, K. D. (1987). A simple, positive semi-definite, heteroskedasticity and autocorrelation consistent covariance matrix. *Econometrica*, 55(3), 703–708.